

Electronic Thesis and Dissertation Repository

---

10-26-2015 12:00 AM

## Feasibility of using Arterial Spin Labeling for Detecting Longitudinal Changes in Cerebral Blood Flow

Tracy Ssali  
*The University of Western Ontario*

Supervisor  
Dr Keith St Lawrence  
*The University of Western Ontario*

Graduate Program in Medical Biophysics  
A thesis submitted in partial fulfillment of the requirements for the degree in Master of Science  
© Tracy Ssali 2015

Follow this and additional works at: <https://ir.lib.uwo.ca/etd>



Part of the [Biochemistry, Biophysics, and Structural Biology Commons](#), [Diagnosis Commons](#), [Medical Biophysics Commons](#), and the [Other Analytical, Diagnostic and Therapeutic Techniques and Equipment Commons](#)

---

### Recommended Citation

Ssali, Tracy, "Feasibility of using Arterial Spin Labeling for Detecting Longitudinal Changes in Cerebral Blood Flow" (2015). *Electronic Thesis and Dissertation Repository*. 3319.  
<https://ir.lib.uwo.ca/etd/3319>

This Dissertation/Thesis is brought to you for free and open access by Scholarship@Western. It has been accepted for inclusion in Electronic Thesis and Dissertation Repository by an authorized administrator of Scholarship@Western. For more information, please contact [wlsadmin@uwo.ca](mailto:wlsadmin@uwo.ca).

FEASIBILITY OF USING ARTERIAL SPIN LABELING FOR DETECTING  
LONGITUDINAL CHANGES IN CEREBRAL BLOOD FLOW

(Thesis format: Monograph)

by

Tracy Ssali

Graduate Program in Medical Biophysics

A thesis submitted in partial fulfillment  
of the requirements for the degree of  
Masters of Science

The School of Graduate and Postdoctoral Studies  
The University of Western Ontario  
London, Ontario, Canada

© Tracy Ssali 2015

## Abstract

The ability of the perfusion MRI technique, arterial spin labeling (ASL), to quantify cerebral blood flow (CBF) makes it attractive for longitudinal studies of changes in brain function, such as those related to chronic pain. However, ASL's poor spatial resolution makes image alignment between sessions difficult, leading to increased variance and greater Type-I errors. In addition, variability due to differences in basal blood flow between sessions and confounding effects such as the arterial transit time (ATT) have the potential to reduce reproducibility over time. The focus of this thesis is to investigate the ability of ASL to detect long-term changes in regional CBF within an individual on a voxel-wise level. It is hypothesized that ASL has the sensitivity to detect activation-induced CBF changes over periods as long as a month if the sources of variance that degrade between-session comparisons are minimized. To test this hypothesis rest and activation (motor task) CBF images were acquired from healthy subjects on three separate imaging sessions. Registration errors were minimized by using individual head molds to replicate the head position in successive sessions. Variations in resting CBF were controlled for by performing the imaging during the same time of day, and subjects were asked to refrain from using common substances, such as caffeine, that are known to affect CBF. Finally, ATT maps were generated on each session to investigate its stability. From these data sets, the within- and between-session variability in CBF was determined and motor-related activation maps were generated from rest and activation data acquired on from the same session and from sessions separated by a week and a month. The results demonstrated excellent reliability (intraclass correlation coefficients greater than 0.75) both within- ( $0.89 \pm 0.2$ ) and between-session ( $0.84 \pm 0.15$ ), and high reproducibility (within subject coefficient of variation, wsCV, greater than 20%) within- (wsCV =  $4.7 \pm 4.5\%$ ) and between-session (wsCV =  $5.7 \pm 4.4\%$ ). Between-session reproducibility of the ATT was high (wsCV =  $5.0 \pm 2.7\%$ ), suggesting that the confounding effect of ATT over a month was minimal. The similarity in within- and between-session variability and their activation maps indicated that registration errors between sessions were minimal. Measures of precision of activation demonstrated that less than ~20% of between-session activation were false positives. These results demonstrate the feasibility of conducting voxel-wise analysis of CBF images acquired on different days and highlight the potential of this technique for longitudinal studies.

## Keywords

Arterial Spin Labeling, Cerebral Blood Flow, Arterial Transit Time, Reproducibility, Reliability, Precision, Longitudinal Activation

## Acknowledgments

This thesis wouldn't be possible without the guidance and support of my supervisor, Dr. Keith St Lawrence. Keith has been an inspiring role model and mentor to me from whom I've learned so much. I am fortunate to have an advisor who was available to provide me with the guidance I needed and the freedom to explore new ideas.

Thank you to my advisory committee, Dr. Terry Thompson and Dr. Ravi Menon for their insightful advice and mentorship.

To my lab mates, Udunna Anazodo and Mahsa Shokouhi, I truly appreciate your guidance and advice. Your contagious enthusiasm brightened the research environment.

Finally, I would like to thank my family for all the love and support they have given me over the years. Mom and Dad, thank you for your continuous encouragement. Ashley, Denise and Laureena you are the best sisters I could ever ask for. Thank you for believing in me.

Tracy Ssali

November 2015

# Table of Contents

Abstract .....	ii
Acknowledgments.....	iv
Table of Contents .....	v
List of Tables .....	viii
List of Figures .....	ix
List of Appendices .....	x
List of Abbreviations .....	xi
Chapter 1 .....	1
1 Introduction .....	1
1.1 Clinical Relevance: Chronic Pain .....	1
1.2 Modern Neuroimaging.....	3
1.3 Arterial Spin Labeling.....	6
1.3.1 Overview.....	6
1.3.2 Labeling Schemes .....	7
1.3.3 Cerebral Blood Flow Quantification Model .....	9
1.3.4 Confounds to Cerebral Blood Flow Quantification .....	11
1.4 Reproducibility, Reliability and Precision Measurements.....	14
1.5 Longitudinal Studies .....	17
1.5.1 Longitudinal Studies with ASL: Challenges and Previous work.....	17
Chapter 2.....	24
2 Methods.....	24
2.1 Study Design.....	24
2.1.1 Activation Paradigm .....	25
2.1.2 Arterial Transit Time Imaging .....	27

2.2	Volunteers .....	27
2.3	Between-Session Variability.....	28
2.4	Data Acquisition .....	29
2.5	Image Processing and Analysis .....	30
2.5.1	Perfusion-Weighted Imaging.....	30
2.5.2	Arterial Transit Time Images.....	32
2.6	Reproducibility of Arterial Spin Labeling .....	33
2.6.1	Variability in Resting Cerebral Blood Flow .....	33
2.6.2	Variability in Arterial Transit Time.....	34
2.6.3	Motor Activation.....	35
Chapter 3	.....	37
3	Results .....	37
3.1	Study Demographics .....	37
3.2	Alignment of Images.....	37
3.3	Analysis of Resting Cerebral Blood Flow .....	39
3.3.1	Mean Resting Blood Flow .....	39
3.3.2	Reproducibility of Resting Blood Flow .....	40
3.3.3	Reliability of Resting Blood Flow .....	43
3.4	Arterial Transit Time Reproducibility .....	44
3.5	Reproducibility of Motor Task Activation .....	46
3.6	Precision of Motor Activation .....	48
Chapter 4	.....	50
4	Discussion .....	50
Chapter 5	.....	57
5	Summary .....	57
5.1	Limitations and Future Work.....	57

5.2 Conclusion .....	59
References .....	60
Appendices.....	72
Curriculum Vitae .....	75



## List of Tables

Table 3.1: Scan times for each subject.....	37
Table 3.2: Mean translation and rotation parameters.....	39
Table 3.3: Mean resting CBF (ml/100g/ml) in select ROIs (N = 7). ....	40
Table 3.4: Mean voxel-wise wsCV for absolute and relative resting CBF in select ROIs.....	42
Table 3.5: Mean voxel-wise ICC for absolute and relative resting CBF in select ROIs .....	44
Table 3.6: Percent CBF change in the motor cortex during finger tapping .....	48

## List of Figures

Figure 1.1: Comparison of general characteristics of nuclear imaging techniques .....	3
Figure 1.2: Schematic of (A) PASL, (B) CASL and PCASL labeling schemes .....	8
Figure 1.3: pCASL fractional signal as a function of time. ....	13
Figure 1.4: Depiction of precision measurement. ....	16
Figure 1.5: Talairach normalized group activation maps of motor task paradigm.....	18
Figure 1.6: Individual subject activation maps for motor-visual activation task.....	22
Figure 2.1: Sequence for sequential finger tapping .....	25
Figure 2.2: Schematic of motor task paradigm.....	25
Figure 2.3: Overview of preprocessing steps.....	31
Figure 2.4: Schematic describing the formation of activation contrasts.....	35
Figure 3.1: T2-weighted images acquired during three imaging sessions.....	38
Figure 3.2: MNI normalized group average mean resting CBF .....	39
Figure 3.3: Relative and absolute voxel-wise wsCV maps.....	41
Figure 3.4: Voxel-wise ICC maps within and between sessions .....	43
Figure 3.5: Group mean ATT maps (in seconds) for each session. (N=7) .....	45
Figure 3.6: Between-sessions and between-subjects reproducibility of arterial transit times.	45
Figure 3.7: Areas of significant CBF increases associated with finger tapping .....	47
Figure 3.8: Precision measurements for each subject.....	49

## List of Appendices

Appendix A: Ethics Approval Notice .....	72
Appendix B: Copyright license for Figure 1.5.....	73
Appendix C: Copyright license for Figure 1.6.....	74

## List of Abbreviations

$^{15}\text{O-H}_2\text{O}$	Radioactive Water
$^{18}\text{F-FDG}$	Fluorodeoxyglucose
$^{99\text{m}}\text{Tc- HMPAO}$	Hexamethylpropyleneamine Oxime Technetium
AAL	Automated Anatomical Labeling
ACA	Anterior Cerebral Artery
aCBF	Absolute Cerebral Blood Flow
AFP	Adiabatic Fast Passage
ANOVA	Analysis of Variance
ASL	Arterial Spin Labeling
ATT	Arterial Transit Time
B1	RF Magnetic Field Strength
BET	Brain Extraction Tool
BOLD	Blood Oxygen Dependent
c(t)	Delivery Function
CASL	Continuous Arterial Spin Labeling
CBF	Cerebral Blood Flow
DICOM	Digital Imaging and Communications in Medicine
FABBER	Fast ASL and BOLD Bayesian Estimation Routine
fMRI	Functional Magnetic Resonance Imaging
FP	False Positive
FWHM	Full Width at Half Maximum
G	Gradient Amplitude
GLM	General Linear Model
GRASE	Gradient and Spin Echo
ICC	Intra-Class Correlation Coefficient
m(t)	Decay Function
M0	Equilibrium Magnetization
MCA	Middle Cerebral Artery
MDI	Methylene Diphenyl Diisocyanate
MNI	Montreal Neurological Institute
NifTI	Neuroimaging Informatics Technology Initiative
PASL	Pulsed Arterial Spin Labeling
PC	Phase Contrast
PCA	Posterior Cerebral Artery
pCASL	Pseudo-Continuous Arterial Spin Labeling
PET	Positron Emission Tomography
PLD	Post Labeling Delay
r(t)	Residue Function
rCBF	Relative Cerebral Blood Flow
RF	Radiofrequency
SPECT	Single Photon Emission Computed Tomography

SPM	Statistical Parametric Mapping
T1	Longitudinal Relaxation Time Constant
T1 <sub>a</sub>	T1 of Blood
T1 <sub>t</sub>	T1 of Tissue
T1 <sub>app</sub>	Apparent T1 Decay
T2	Transverse Relaxation Time Constant
T2*	Apparent T2
TE	Echo Time
TP	True Positive
TR	Repetition Time
v	Velocity
wsCV	Within Subject Coefficient of Variance
$\alpha$	Inversion Efficiency
$\gamma$	Gyromagnetic Constant
$\Delta M$	Perfusion Weighted Image
$\lambda$	Blood-Brain Equilibrium Partition Coefficient
$\sigma_{bs}^2$	Between-Subjects Variance
$\sigma_{er}^2$	Error Variance
$\sigma_{se}^2$	Systemic Error Variance
$\tau$	Labeling Duration
$\omega$	Post Labeling Delay

## Chapter 1

### 1 Introduction

#### 1.1 Clinical Relevance: Chronic Pain

In its most benign form, pain is an unpleasant, although necessary short-term sensation that warns of impending or actual tissue damage. When this sensation outlasts the normal time of healing, typically identified as 3-6 months, it is considered chronic and no longer serves a biological purpose<sup>1-3</sup>. Instead, it imposes a burden on the individuals it affects and society. Chronic pain is one of the most prevalent diseases and is a common cause of major disability and economic loss<sup>4</sup>. One in five Canadians suffer from chronic pain and each year it costs over \$6 billion in healthcare costs and over \$37 billion in costs related to job loss and sick days<sup>4-6</sup>. Compared to other chronic medical conditions, individuals suffering from chronic pain face significantly lower quality of life as indicated by short form health surveys (SF-36v2). Upwards of 70% of participants indicated that their condition greatly interfered with their daily routines<sup>7</sup>. Although treatment plans are able to reduce pain intensity by up to 30%, it does not guarantee an improvement in function<sup>8</sup>. In many cases this means that chronic pain sufferers remain unable to regain their former independent lifestyles.

Strategies for treatment and management of pain remain a challenge for health care providers. Since pain is a subjective experience, and in the absence of a biological marker, the primary tool for assessment is self-reports from patients<sup>9</sup>. While multidisciplinary treatment approaches that take social and physiological factors into account help with coping, there is currently an unmet need for novel and efficacious treatments particularly for individuals with intractable pain who already suffer from acute diseases such as cancer, HIV and diabetes<sup>6</sup>. Treatment of pain has become heavily reliant

on opioids for temporary relief which are addictive and have serious side effects. A recently published review identified that over the past 25 years the steady increase in dose, volume and prevalence of opioids among chronic pain sufferers and has led to an overall increase in deaths related to opioid overdoses <sup>10</sup>. Given these unsettling facts, there is growing need to better understand the underlying causes of chronic pain and determine potential targets for therapeutic interventions. Functional neuroimaging is a powerful tool for noninvasively mapping brain activity and has shown promise in pain research <sup>11</sup>.

Perception of acute pain involves the transfer of nerve impulses from the peripheral nociceptors to the central nervous system and into the brain where these impulses directed to various regions based on intensity and bodily location of the painful stimulus. This process has led to the theory that plasticity of the central nervous system plays a role in the development and maintenance of chronic pain <sup>12</sup>. Unlike the bottom-up state of acute pain where sensory pain information dominates, chronic pain is believed to be a top-down state governed by cognitive factors. This was confirmed by neuroimaging studies which report a strong correlation between alterations in thalamic activity and duration of chronic pain <sup>13,14</sup>. Long term chronic pain patients had decreased thalamic activity, suggesting an adaptive top-down response whereas those with early onset of chronic pain had increased thalamic activity, coinciding with the sensory pathway of pain processing in healthy individuals.

The vast majority of pain studies have primarily focused on activation related to stimulated pain <sup>11,15-17</sup>. More recently, studies have been investigating the ongoing or chronic pain state <sup>18,19</sup>; however, to date no studies have investigated functional changes in the brain related to progression of acute-to-chronic pain. Being able to quantify these changes would provide a better understanding of how the duration of pain affects the

brain and, more importantly, treatment efficacy. That is, can we discriminate between treatment responders and non-responders based on differences in brain activity related to their current pain state? Answering this question will require a functional imaging method capable of longitudinal monitoring. Ideally the technique would have the sensitivity to monitor changes in individual patients considering the large variability in treatment response. Towards this goal, this thesis will focus on investigating a method for detecting long-term changes in cerebral blood flow.

## 1.2 Modern Neuroimaging

The predominant brain mapping methods being used currently are based on the coupling between neuronal activity and regional cerebral blood flow (CBF). These neuroimaging techniques can be broadly categorized into nuclear medicine and functional magnetic resonance imaging (fMRI) methods. Nuclear imaging techniques consist of positron emission tomography (PET) and single photon emission computed tomography (SPECT), while fMRI encompasses blood oxygen dependent (BOLD) and arterial spin labeling (ASL) <sup>20</sup>.

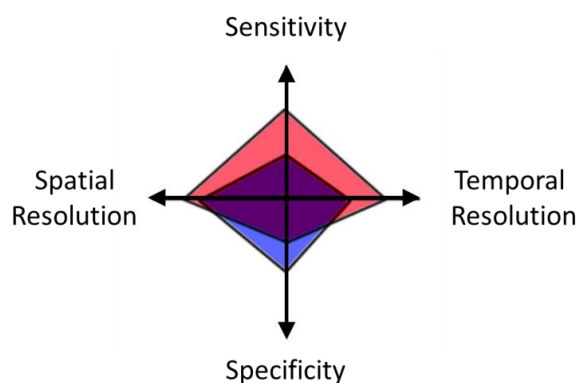


**Figure 1.1:** Comparison of general characteristics of nuclear imaging techniques (PET/SPECT), shown in blue, and functional MRI technique (BOLD), shown in pink. Areas of overlap are shown in purple.



Each approach bears strengths and weaknesses, making them better suited for different applications (Figure 1.1). Nuclear perfusion imaging techniques involve measuring the uptake of an injected radioactive tracer. Based on the pharmacokinetics of the tracer, detected regional activity distribution will reflect various biological parameters. To measure CBF, PET uses radioactive water ( $^{15}\text{O-H}_2\text{O}$ ) whereas gamma emitting hexamethylpropyleneamine oxime *technetium* ( $^{99\text{m}}\text{Tc-HMPAO}$ ) is a commonly used SPECT flow tracer. The utility of PET and SPECT stems from their abilities to detect nanomoles of tracer with high sensitivity and specificity in absolute units <sup>21</sup>. However, exposure to ionizing radiation and the half-life of the tracer limits the number of measurements acquired per subject. This limits voxel-wise analysis, or statistical parametric mapping (SPM), to either group analysis or a template-based approach <sup>22,23</sup>. For the purposes of tracking disease progression within a single subject, this approach is suboptimal because the detected activity depends on the control template and the accuracy of spatial normalization <sup>24</sup>. For example, in a PET study comparing glucose metabolism patterns in Alzheimer's disease patients to healthy controls, the extent and localization of regions demonstrating metabolic changes varied based on whether a common  $^{18}\text{F-FDG}$  PET or  $^{15}\text{O-H}_2\text{O}$  PET template was used to spatially normalize the data <sup>25</sup>. These artifacts or false positives due to normalization can introduce ambiguities into the final interpretation of the results. Additionally, modeling tracer kinetics required for CBF quantification is an involved and invasive process as the time-dependent variation in the radioactivity in the arterial blood needs to be measured by collecting arterial blood samples. This is both time consuming and sensitive to error, making it difficult to justify for routine imaging. To avoid arterial sampling, the arterial input function can be estimated based a population-based input function <sup>26,27</sup>. However, the shape of the arterial input will vary based on the disease group and the radioactive tracer being used, introducing variability in CBF estimations. Alternatively, a semi-quantitative

approach may be implemented by intensity normalizing signals to a global mean at the expense of reduced accuracy<sup>28,29</sup>.

FMRI is a more popular technique for functional imaging as it offers a safe and non-invasive approach to measuring brain function. The dominant method using BOLD contrast is based on the change in the oxyhemoglobin concentration caused by an increase in CBF<sup>30</sup>. Deoxyhemoglobin is a paramagnetic molecule that produces a susceptibility induced field change, resulting in a decrease in the apparent transverse relaxation time constant ( $T2^*$ )<sup>31,32</sup>. Oxyhemoglobin, on the other hand, is diamagnetic<sup>33</sup>. With increased brain activity, the amount of oxyhemoglobin relative to deoxyhemoglobin increases due to the increase in CBF. This results in a local increase in  $T2^*$ . While BOLD has become the standard neuroimaging method, low frequency baseline signal drifts reduce its sensitivity if the spacing between the baseline and stimulus is greater than a few minutes<sup>34,35</sup>. In addition, BOLD contrast is a relative signal change and consequently the technique is not suitable for monitoring across imaging sessions<sup>36</sup>.

The stability of the ASL signal combined with being non-invasive, unlike PET and SPECT, and quantifiable, unlike BOLD, makes it ideal for studying long-term changes in brain activity. The unique feature that separates ASL from the other functional neuroimaging techniques is that arterial blood water is used as an endogenous diffusible tracer. Image contrast is based on the changes in brain tissue signal due to the increase or decrease in tracer concentration. Since subjects are not exposed to ionizing radiation, the technique is well suited to repeated scanning<sup>37</sup>. This is advantageous in populations (e.g. pediatric or renal disease) where the use of radioactive tracers poses a large risk<sup>38</sup>. In relation to BOLD, ASL provides greater spatial localization. The spatial correlation of the BOLD signal to the site of activation is relatively poor since more than 65% of the BOLD signal is accounted for by intravascular spins<sup>39</sup>. In contrast, the ASL signal reflects tracer

delivered to the tissue. Consequently, in theory ASL reflects regional changes in activity with greater sensitivity. Furthermore, since CBF is in theory insensitive to scanning parameters, in addition to the traditional detection of global hypo and hyperperfusion, it permits comparison of multiple measurements in a longitudinal study<sup>40</sup>.

## 1.3 Arterial Spin Labeling

### 1.3.1 Overview

As previously alluded to, ASL signal contrast is generated by magnetically labeling the blood flowing into the tissue of interest<sup>41</sup>. Following a short delay to allow the labeled blood water to reach the imaging plane, an image that contains signal from labeled water and static tissue is acquired. To remove the static tissue contribution, a second image, known as the control, is acquired using the same imaging parameters, but without the arterial labeling. Control and tag images are acquired in interleaved succession. Subtraction of the control-tag pairs results in perfusion weighted or difference images ( $\Delta M$ ) that are directly proportional to CBF<sup>42</sup>.

The magnitude of the signal difference is dependent on the lifetime of the labeled blood water - i.e., the longitudinal relaxation time of blood,  $T1_a$  (1300 – 1750 ms); the amount of time it takes for the labeled blood water to reach imaging voxels, which is referred to as the arterial transit time (ATT) (800 – 1200 ms); and blood flow<sup>43</sup>. Since the ATT and  $T1_a$  are similar in magnitude, the signal change is typically only 0.5 - 1% of equilibrium magnetization, resulting in a poor signal-to-noise ratio (SNR)<sup>38</sup>. To improve the SNR, ASL images are acquired at relatively low resolution (4 x 4 x 6 mm<sup>3</sup> voxel) and multiple control-tag pairs are acquired for signal averaging<sup>44</sup>. In a study by Gevers et al., it was estimated that 20 control-tag pairs are required to obtain steady and reproducible CBF values<sup>45</sup>. Although, to improve the SNR, it is not uncommon to acquire upwards of 40

images<sup>38,46</sup>. A second limitation of ASL is its temporal resolution. To obtain a single perfusion weighted image, two images, namely the control and label, are required. Since repetition times range between 2 – 4 seconds, perfusion weighted images are acquired every 4 – 8 seconds<sup>43</sup>. This makes ASL less suitable for detecting fast changes in the brain. In addition, it can lead to increased sensitivity to gross head motion and physiological motion<sup>47</sup>. With emerging methods such as single-shot ASL, where control and tag images are acquired after a single labeling period, and phased array receiver coils which can be optimized for parallel imaging, scan time can be reduced<sup>48</sup>.

Clinically, ASL imaging has been used to study conditions including, but not limited to chronic pain<sup>17,49</sup>, Alzheimer's disease<sup>50,51</sup>, stroke and carotid occlusive diseases<sup>52,53</sup>. In addition to its clinical applications, ASL has provided valuable information regarding physiology in healthy individuals<sup>54,55</sup> and drug development<sup>56-58</sup>. It has been demonstrated that ASL has the sensitivity to detect relevant changes in CBF within an individual. For example, in a study assessing activation related to experimental pain, ASL was able to detect as small as a 2.2% change in CBF within an individual<sup>15</sup>. Furthermore, ASL has been validated against PET perfusion imaging, the gold standard method of CBF measurement<sup>59-61</sup>.

### 1.3.2 Labeling Schemes

Depending on the duration and spatial extent of signal inversion, labeling strategies are classified as pulsed (PASL), continuous (CASL) or pseudo-continuous (pCASL) (Figure 1.2). With PASL, a large volume of tissue (10-20 cm) proximal to the imaging slice is labeled using a short (5 – 25 ms) inversion radiofrequency (RF) pulse<sup>62-64</sup>. With CASL, a continuous off-resonance RF pulse, typically 1 – 3 s, is applied in the presence of weak gradient to invert the magnetization of arterial blood flowing through a labeling plane perpendicular to the feeding artery<sup>38,65</sup>. This process is known as adiabatic fast passage

(AFP). In the presence of an applied magnetic gradient, the resonant frequency is spatially dependent and the blood magnetization experiences a frequency sweep as it flows through the labeling plane. For a high inversion efficiency, denoted  $\alpha$ , blood passing through the plane needs to meet the adiabatic condition:  $1/T_1, 1/T_2 \ll Gv/B_1 \ll \gamma B_1$ <sup>66</sup>, where  $T_1$  is the longitudinal relaxation rate,  $T_2$  is the transverse relaxation rate,  $G$  is the gradient amplitude,  $v$  is the velocity of blood along the direction of the gradient,  $B_1$  is the strength of the RF magnetic field and  $\gamma$  is the gyromagnetic constant. The strength of the applied gradient and RF are chosen based on the typical range of velocities found in the carotids.

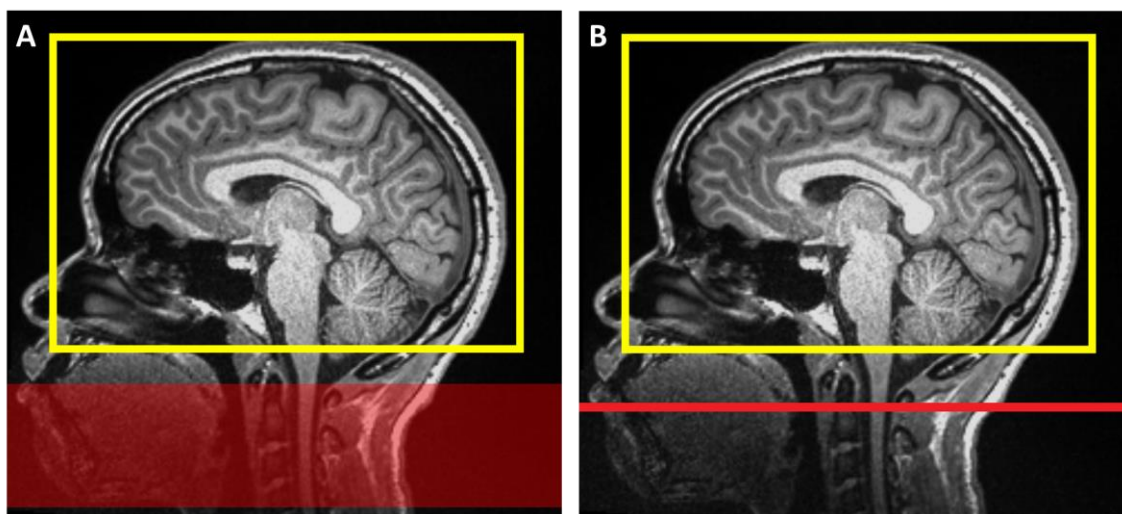


**Figure 1.2:** Schematic of (A) PASL, (B) CASL and PCASL labeling schemes overlaid on a sagittal human brain. PASL inversion of blood and tissue signal occurs in the thick band shaded in red. For CASL/PCASL, inversion takes place as blood passes through the thin red band.

PASL offers high labeling efficiency, since unlike CASL, signal inversion is not sensitive to the velocity of blood within the labeling volume<sup>44</sup>. However, the SNR for PASL is less than for CASL because the in-flowing arterial blood is only labeled once and this magnetization quickly decays with  $T_{1a}$ . Despite the improved SNR achieved using

CASL, this approach is difficult to implement due to the off-resonance irradiation of large macromolecules in the tissue <sup>67</sup>. The magnetization transfer between this bound pool and tissue water produces an unwanted signal change that is much greater than the ASL signal and, therefore, must be carefully controlled. One approach is to use a separate RF coil for labeling, but this is technically more complicated <sup>68</sup>.

To address the limitations of CASL, pCASL, the current recommended labeling strategy, was developed by Alsop et al. <sup>43,69</sup>. Conceptually, this approach is identical to CASL, except in lieu of a continuous pulse, a series of short RF pulses (1 pulses/ms) are applied <sup>69</sup>. This labeling scheme results in reduced magnetization transfer effects <sup>43,44,69</sup>. Pseudo-CASL is easily implemented on conventional 1.5/3 T MRI scanners and has been quickly adopted in the ASL community.

### 1.3.3 Cerebral Blood Flow Quantification Model

To quantify CBF in standard units of flow (i.e., mL of blood/100g of tissue/min), perfusion weighted images are incorporated into the general kinetic model. The general kinetic model describes the kinetics of  $\Delta M$  as the delivery function  $c(t)$ , the residue function or the clearance of labeled blood from the voxel  $r(t)$ , and the recovery of the longitudinal magnetization in the tissue  $m(t)$  <sup>70</sup>. For pCASL, the delivery function is given by the piecewise function:

$$c(t) = \begin{cases} \mathbf{0} & \mathbf{0} < t < ATT \\ \alpha e^{\frac{-t}{T_{1a}}} & ATT < t < \tau + ATT \\ \mathbf{0} & \tau + ATT \leq t \end{cases} \quad (1.1)$$

where  $ATT$  is the arterial transit time,  $T_{1a}$  is the longitudinal relaxation of arterial blood,  $\alpha$  is the labeling efficiency and  $\tau$  is the labeling duration. As demonstrated in this

equation, the delivery of label the tissue is dependent on the ATT, which will be discussed further in the following sections. Following labeling, the labeled magnetization in tissue decays at:

$$m(t) = e^{-\frac{t}{T_1}} \quad (1.2)$$

where  $T_1$  is the longitudinal relaxation of tissue. Assuming single compartment kinetics,  $r(t)$  is given by:

$$r(t) = e^{-\frac{ft}{\lambda}} \quad (1.3)$$

where  $f$  is the CBF in mL/100g/min, and  $\lambda$  is the blood-brain partition coefficient of water (assumed to be 0.9 mL/g). Since arterial blood water diffuses from the blood into the tissue,  $\lambda$  represents the equilibrium ratio of the water concentration in tissue and blood. Although, it varies slightly based on tissue type, error encountered by assuming a single value is less than 10%<sup>43,71</sup>. The difference signal is the convolution of the input function with the tissue response. Mathematically,

$$\Delta M = 2M_0 f \{c(t) * [r(t)m(t)]\} \quad (1.4)$$

Assuming instantaneous exchange of labeled water from the microvasculature to the surrounding tissue, the analytical solution to the convolution or the difference in magnetization as a function of time is a stepwise function:

$$\Delta M(t) = \frac{2\alpha M_0 f T_{1app}}{\lambda} e^{-\frac{ATT}{T_{1a}}} \begin{cases} 0 & 0 < t < ATT \\ 1 - e^{-\frac{-(t-ATT)}{T_{1app}}} & ATT < t < \tau + ATT \\ e^{-\frac{-(t-ATT-\tau)}{T_{1app}}} \left(1 - e^{-\frac{-\tau}{T_{1app}}}\right) & \tau + ATT \leq t \end{cases} \quad (1.5)$$

where  $M_0$  is the equilibrium magnetization of tissue and  $T_{1app}$  is called the apparent T1, and is given by:

$$\frac{1}{T_{1app}} = \frac{1}{T_{1t}} + \frac{f}{\lambda} \quad (1.6)$$

Considering that T1 of grey matter and blood are similar in values and  $f/\lambda$  is quite small, it is not unreasonable to assume that  $T_{1a}$  is approximately equal to  $T_{1app}$ . Using this assumption, CBF can be determined from Equation (1.5). For the condition that the PDL  $>$  ATT, CBF is given by:

$$f = \frac{\Delta M \lambda e^{\frac{PLD}{T_{1a}}}}{2\alpha M_0 T_{1a} \left( 1 - e^{\frac{-(\tau + PLD)}{T_{1a}}} \right)} \quad (1.7)$$

### 1.3.4 Confounds to Cerebral Blood Flow Quantification

Equation (1.7) demonstrates that the relationship between  $\Delta M$  and CBF depends on the proton density or equilibrium magnetization ( $M_0$ ),  $T_{1a}$ , labeling efficiency, and ATT.  $T_{1a}$ , labeling efficiency and ATT can be based on values from the literature; however, variability between subjects and variations across brain regions in terms of ATT can lead to errors in the calculated CBF.

The relaxation rate of the tracer depends on its local environment. Consequently, once the label diffuses from the blood into the tissue, the relaxation rate shifts from the T1 of blood ( $T_{1a}$ ) to the T1 of tissue ( $T_{1t}$ ). The one compartment model assumes that  $T_{1a}$  and  $T_{1t}$  are similar. However, if they are not, assigning a one compartment model can lead to a ~20% overestimation in grey matter perfusion <sup>72</sup>. An alternate approach which avoids the need for measuring  $T_{1t}$ , is to set the acquisition window such that images are acquired after the label reaches the microvasculature but before the label diffuses into the tissue.



Since the signal remains intravascular, the single compartment model is able to provide a robust estimate of CBF<sup>40</sup>.

The second confound to measuring CBF is variations in labeling efficiency. The labeling efficiency refers to the efficiency of the adiabatic inversion of arterial blood water. In pCASL,  $\alpha$  is assumed to be 85%<sup>69</sup>. However, due to magnetic field inhomogeneities and blood velocities outside the optimal range (10 – 60 mL/100g/min), this value may be lower than this literature value<sup>40,73</sup>. The labeling efficiency can be measured with phase contrast (PC) MRI. PC is a non-invasive technique for which applies a gradient to induce a phase shift in moving protons. The signal intensity reflects the direction and speed of the protons. To estimate the labeling efficiency, PC images of the feeding arteries of the brain acquired over one cardiac cycle are used to measure the CBF volume (mL/min). The ratio of the CBF volume measured with PC and the CBF volume measured with ASL (i.e. cerebral volume from a T1-weighted image and CBF from ASL) gives the labeling efficiency<sup>40</sup>. Since errors in the labeling efficiency calculation is reflected as a systemic shift in global CBF, for studies assessing changes in CBF, all images will be affected in the same manner and therefore will not affect the end result. Consequently, in this situation, measurement of the labeling efficiency is not essential.

A third confound to accurate CBF quantification is the dependency of the ASL signal on the ATT. The ATT represents the time required for labeled blood water to move from the labeling plane to an imaging voxel. To reduce the influence on ATT on the  $\Delta M$  signal, Alsop et al., introduced the concept of introducing a delay between the end of the labeling period and the start of image acquisition (i.e. the PLD) to allow all of the labeled water to reach the imaging volume<sup>74</sup>. The challenge with this approach is selecting the optimal PLD. That is, if the PLD is too short, CBF will be underestimated as the labeled blood has not fully reached the imaging plane, whereas long PLDs lead to substantial

signal loss due to T1 decay. While the choice of PLD can be selected from previous studies in which the ATT was directly measured, there are variations due to age, gender, pathology and within different vascular territories in the brain <sup>75</sup>. For example, older individuals, the age bracket where chronic pain is most prevalent <sup>2</sup>, have long ATTs (~1200 ms) as the vessels in the brain becomes more are tortuous <sup>43</sup>. Additionally, within all individuals, there are increased ATT in white matter, water shed regions or vascular border zone regions <sup>75</sup>.

Given these facts, measurement of the ATT can improve the accuracy of CBF measurements. The interdependence between the ATT and the ASL signal allows for the measurement of ATT. As shown in Figure 1.3 and Equation (1.5), the ASL signal consists of 3 parts. The first period is the time when the labeled blood has not reached the imaging voxel and therefore the signal is equal to zero.

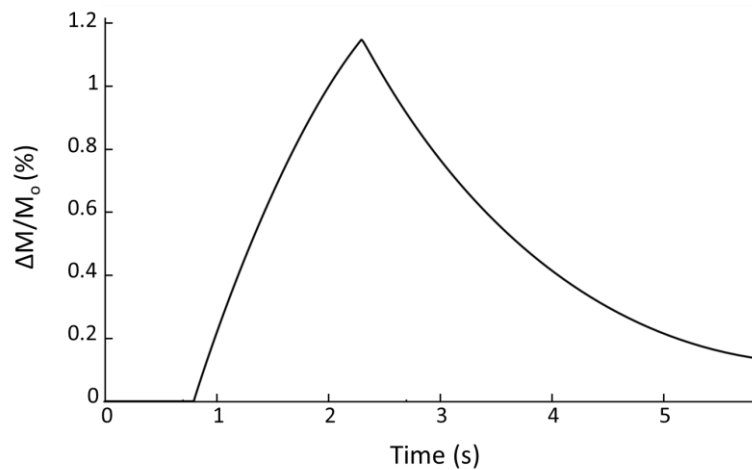


**Figure 1.3:** pCASL fractional signal as a function of time. The plot was generated using Equation (1.5) and the following parameters:  $\alpha = 85\%$ ,  $\text{CBF} = 60 \text{ mL}/100\text{g}/\text{min}$ ,  $T1_a = T1_{app} = 1650 \text{ ms}$ ,  $\text{ATT} = 800 \text{ ms}$ ,  $\lambda = 0.9 \text{ mL}/\text{g}$  and  $\tau = 1500 \text{ ms}$ .

As the inflowing labeled blood water reaches the imaging voxel or tissue, the signal increases. Finally as the signal decays, the signal decreases. By acquiring ASL images at multiple PLDs and fitting the fractional signal to Equation (1.5), the ATT can be estimated. Current strategies proposed for measuring ATT, such as those involving blood flow crusher gradients or multiple PLDs, tend to be time consuming, suffer from low SNR and contamination from intravascular signals; thus, leading to inaccurate measurements<sup>76</sup>. A second approach is to use a relatively low resolution ASL sequence. ATT images are fundamentally low resolution since variations are based on large vascular territories<sup>76</sup>. By increasing the voxel size, the time required to acquire ATT images is greatly reduced.

## 1.4 Reproducibility, Reliability and Precision Measurements

Analysis of measurement error is an important step towards the widespread use of a new technique. Reliability refers to the magnitude of error variance relative to “true” and inherent variability between subjects. In other words, it expresses the consistency of test and retest measurements made at different time points. Reliability is measured using the intra-class correlation coefficient (ICC)<sup>77</sup>. Although there are six versions, the most basic form of the ICC is given by the ratio between the between-subjects ( $\sigma_{bs}^2$ ) variance and the total variance (or the sum of between subject variance and the error variance ( $\sigma_{er}^2$ ):

$$ICC = \frac{\sigma_{bs}^2}{\sigma_{bs}^2 + \sigma_{er}^2} \quad (1.8)$$

In a repeated measures design or a two way mixed model design, error variance is considered to come from one of two sources: systematic error ( $\sigma_{se}^2$ ), or error due to bias in the repeated measures, and random error ( $\sigma_{er}^2$ ), or error due to chance factors<sup>77</sup>. Taking these into account, the ICC becomes:

$$ICC = \frac{\sigma_{bs}^2}{\sigma_{bs}^2 + \sigma_{se}^2 + \sigma_{er}^2} \quad (1.9)$$

ICC values vary from 0 to 1 where values closer to 1 represent greater agreement between measurements. As a general guideline,  $ICC < 0.4$  is denoted as poor,  $0.4 - 0.59$  as fair,  $0.60 - 0.74$  as good, and  $> 0.75$  as excellent <sup>78</sup>. A notable weakness of using the ICC as a measure of reliability is that it is dependent on the variability between subjects in the sample. For example, populations with low between-subject variability will have artificially deflated ICC values relative to a group with high between subject variability even if the variability between repeated measures is small <sup>79,80</sup>. Consequently, it is difficult to generalize results as ICC will vary based on the population. For this reason, it is beneficial to assess the reproducibility in conjunction with reliability.

Reproducibility is defined as the variation in repeated measures from the same subject under changing conditions <sup>81</sup>. In the ASL literature, it is common to use the reproducibility to assess variability in resting blood flow or activation patterns from data acquired on different days <sup>82,83</sup>. If the variation between measurements is low, despite the changing conditions, the reproducibility will be high. Reproducibility is measured using the within subject coefficient of variation (wsCV). WsCV is the ratio of the standard deviation of the difference between repeated CBF measurements to the mean CBF <sup>84</sup>. Mathematically it is given by:

$$wsCV = \frac{SD_{\Delta CBF}}{Mean_{CBF}} \cdot 100 \quad (1.10)$$

where  $SD_{\Delta CBF}$  is the standard deviation of the difference in CBF. WsCV ranges from 0 – 100%. As a general guideline, wsCV below 20% are considered to be within the normal range of ASL studies <sup>85</sup>. One of the advantages of the wsCV is that it is a normalized

parameter and therefore does not depend on the population being studied. This allows for comparisons across studies.

Precision, also known as the positive predictive value is a commonly used metric used to assess the ability of a technique to correctly identify relevant information. The precision is defined as the ratio of the number of correctly predicted positive cases to the total number of predicted positive cases. Mathematically precision is given by:

$$\textit{Precision} = \frac{TP}{TP + FP} \cdot 100 \quad (1.11)$$

where TP represents the amount of true positives and FP represents the number of false positives<sup>86</sup>. Precision can be used to quantitatively assess the extent of false positives in activation maps.

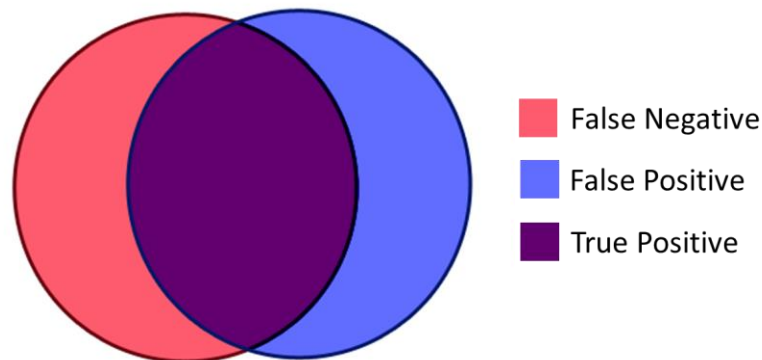


**Figure 1.4:** Depiction of precision measurement. The region shaded in: pink represents false negatives, blue represents the false negatives and purple represents true positives.

As shown in Figure 1.4, the precision would be the ratio of the purple region to the total area of the blue and purple region. Precision ranges from 0 – 100%, where higher values indicate fewer false positives and thus greater similarity between the detected activation and the true activation.

## 1.5 Longitudinal Studies

Knowledge regarding brain function in healthy and chronic pain patients originates from cross-sectional functional neuroimaging studies <sup>19,87,88</sup>. In general, data are compared across groups that differ in the variable of interest, but bear great similarity otherwise. For example, to assess regions associated with pain, chronic pain patients are compared to age-matched healthy controls <sup>87</sup>. However, to investigate the plasticity of the brain, simple comparison of controls against patients is not enough. Convergent evidence from cross-sectional studies indicates that there are changes in brain activity related to the duration of the disease process <sup>13,14</sup>. In addition, these conclusions represent a nomothetic generality and can misrepresent processes which occur in a single individual <sup>89,90</sup>. For these reasons, it would be beneficial to test and confirm these hypotheses with longitudinal studies. Longitudinal studies present a more direct, idiographic measurement of process-related changes that recognizes individual differences. The distinguishing feature of longitudinal studies is that subjects are observed repeatedly allowing for direct assessment of slow changes in CBF over time. Since each subject serves as their own control, confounding effects, such as differences in age and gender no longer confound the results. This allows for studying not only chronic pain, but processes that impede and affect normal development as well as the progression of other pathologies.

### 1.5.1 Longitudinal Studies with ASL: Challenges and Previous work

As explored in Section 1.2, primarily attributed to its insensitivity to task frequency, ASL is arguably the best tool at our disposal for longitudinal neuroimaging of changes in brain function. In addition to being non-invasive, the quantitative feature of ASL – namely its ability to measure CBF – makes it well suited for comparing functional data acquired in separate imaging sessions <sup>34</sup>. This was originally demonstrated by Wang et al., who compared the ability of BOLD and ASL to detect brain activity generated from

alternating rest and finger tapping periods that were separated by 0.5, 1, 2.5, 5, 10, 20 minutes, 1 and 24 hours<sup>34</sup>. Shown in Figure 1.5 are the BOLD group t-maps corresponding to intervals of 30 s and 1 h. These images demonstrated the expected robustness of the BOLD signal when rest and task are separated by 30 seconds; however, the activation disappears when the rest and task epochs are acquired in different sessions separated by 1 hour<sup>91</sup>. In contrast, activation was detected by ASL at both time intervals, including a separation of 24 hours; although the statistical power appears to decrease as the separation increased, as indicated by the decrease in cluster size.

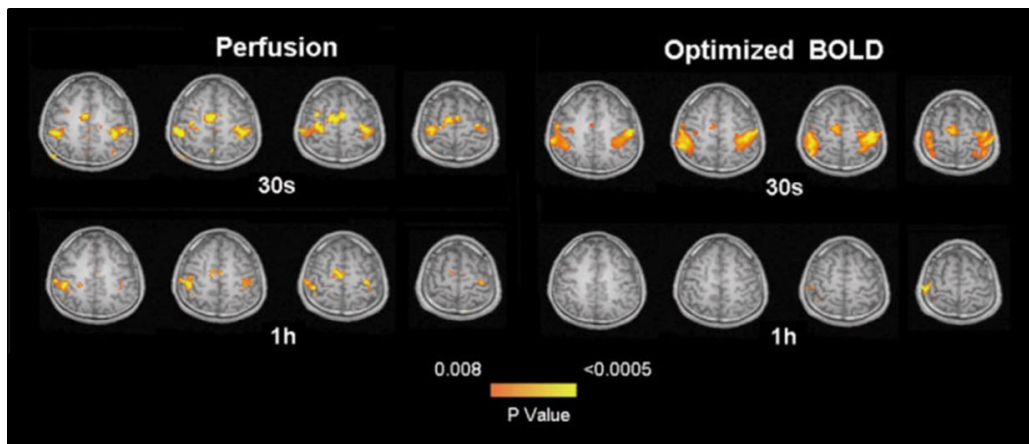


**Figure 1.5:** Talairach normalized group activation maps of motor task paradigm when rest and task were separated 30 s and 1 h with BOLD and perfusion (ASL) imaging. Adapted from Wang et al.<sup>34</sup>.

Since noise analysis was not performed in this study, a question that remains is the sources of variability leading to decreased activation at low task frequency. One possible explanation is that analysis was performed at a group level. Group analysis has decreased sensitivity for detecting differences between states due to the high variability between subjects<sup>92</sup>. There is heavy reliance on the accuracy of the normalization procedure as spatial mismatch of cortical structures reduces the statistical power. In addition because of this high variability, similar to cross sectional studies, this analysis represents a

nomothetic generality, that is, conclusions made from a group study may not apply to individuals.

A second factor is the inherently low SNR of ASL which impedes its sensitivity. When comparing data between sessions, due to the additional sources of variance, the statistical power to detect changes is reduced and therefore the cluster size decreases. Sources of noise in an ASL images can be characterized by scanner and subject noise<sup>93,94</sup>. Scanner noise reflects changes in signal related to: (1) fluctuations in signal caused by temperature dependent motion of electrons (thermal noise) and (2) fluctuations in the functioning MRI hardware including drift and inhomogeneities in the static magnetic field (systemic noise). Subject noise is generally defined as variability in the signal caused by the subject's physiology excluding the neuronal activity of interest<sup>95</sup>.

While each of these can reduce the SNR and thus the reproducibility of the signal, certain features of ASL images mitigate their effects. The signal difference between subsequent control and label pairs is ~1% due to the T1 relaxation of blood. Multiple repetitions are acquired and averaged to ensure a sufficient SNR. This averaging also reduces thermal noise. Systemic noise, in particular drift, is reduced by subtracting control-label pairs<sup>35</sup>. Hence, much of the scanner related noise is small in magnitude can be removed with preprocessing steps<sup>96</sup>. Subject noise within a session can have severe effects on reproducibility of resting CBF. Gross head motion within an imaging session causes blurring which renders the data unusable. With the use of foam to keep the head in place, as is convention, sequences with background suppression, as well as motion correction algorithms and spatial smoothing, this variability can be reduced<sup>43</sup>. Consequently for within-session data, the predominant source of variability is measurement or scanner error, which in most cases is small<sup>97</sup>. Therefore, studies have been able to demonstrate high reproducibility of within-session activation acquired on different days<sup>82,98</sup>.



Variability between sessions on the other hand, is greatly influenced by physiologic factors and therefore it is important to take steps to reduce its influence<sup>85,99,100</sup>. When data are compared between days, additional variability due to transient effects (e.g., mood, arousal, caffeine, food consumption etc.) and between-session co-registration errors due to variability in head positioning in the scanner can result. Previous studies have encouraged subjects to abstain from consuming vasoactive substances and/or scaled the CBF images (e.g. by whole-brain grey matter perfusion), to remove transient changes in global CBF<sup>101,102</sup>. However, scaling needs to be approached with caution as it has the potential to remove relevant variability<sup>102</sup>. Between-session co-registration errors are particularly detrimental in multi-slice acquisitions with gaps between slices. Few studies have assessed the ability of ASL to detect between-session activation, or activation when rest and task are from separate imaging sessions.

A number of studies have assessed the reproducibility and reliability of resting ASL data within time frames ranging from hours<sup>85,97</sup>, weeks<sup>99,103</sup> to months<sup>104</sup>. These studies demonstrated good reproducibility (wsCV < 20%) of resting perfusion. A common finding was that shorter scan intervals had less variability<sup>82,99</sup>. For example, Floyd et al. found that the coefficient of variability was 5.8% when rest periods were separated by an hour and increased to 13% when they were separated by a week<sup>99</sup>. Reproducibility in resting perfusion measured with ASL has also been shown to be comparable to PET<sup>105,106</sup>. In a study by Heijtel et al., it was shown that the repeatability index of CBF measurements between modalities (22.9%) was similar to the between-session repeatability for each modality (i.e. PET (27.6%) and ASL (25.1%)). Since the sources of noise in PET and ASL are different, agreement supports the idea that detected changes are related to biological processes<sup>85</sup>. Among the labeling schemes, pCASL has been shown to have the highest reproducibility<sup>100,102</sup>. This is attributed to its superior SNR relative to PASL and inversion efficiency relative to CASL. Within mean grey matter, the

wsCV within-session, after an hour and after a week were: 3.5%, 5.5% and 8.5% respectively. These figures represent on average a 24% decrease in variability relative to PASL 46% decrease relative to CASL. More recently, studies have shown good reproducibility across multiple centres <sup>103</sup> and multiple vendors <sup>107</sup>. While these studies are a good indication of the applicability of ASL within a clinical setting, all of them focused on region-of-interest (ROI) analysis. ROI analysis is commonly used for both longitudinal and cross sectional assessments of brain function. However, voxel-wise analysis bears greater clinical relevance as regions impacted by the disease may not be known a priori. In addition, accurate delineation of ROIs is performed manually and thus is susceptible to variability between operators, requires experienced personnel and is time consuming <sup>108</sup>.

The few studies that have performed voxel-wise noise analysis of resting CBF demonstrated high correlation between within-session measurements and no significant differences in resting CBF between sessions <sup>102,109</sup>. While baseline variability is an important factor in the detection of activation in longitudinal studies, on its own it is not indicative of the reproducibility of the signal. Inherent noise in both rest and task data introduces uncertainty in regards to what can be considered true activation. Therefore, full characterization of the detection limits can only be accomplished by pairing baseline with task data.

Currently, there are two studies which have conducted a similar line of work. The first study, demonstrated the ability of ASL to detect activation within an individual against a group baseline template <sup>110</sup>. Activation was generated by comparing resting perfusion template created from 25 healthy subjects and activation data from a single subject performing a motor task. Although, activation obtained using the group template and standard general linear model (GLM) analysis were comparable, use of a template is

heavily dependent on the accuracy of the spatial normalization and how well the template characterizes the data <sup>22,24,92</sup>. Therefore, its utility within the context of longitudinal studies is limited. In the second study, using a visually cued motor task (finger tapping), the ability of ASL to detect activation when rest and task were separated by 30 days was compared to activation data generated from rest and task data acquired within the same session <sup>111</sup>.

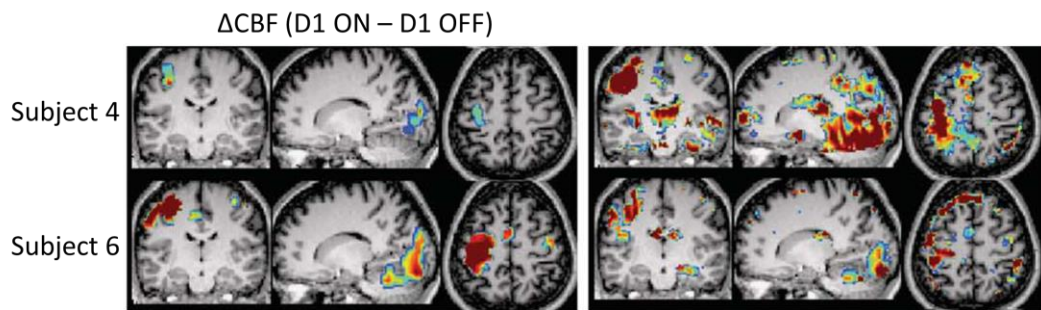


**Figure 1.6:** Individual subject activation maps for motor-visual activation task. Panels to the left are within-session activation, whereas for panels to the right rest and task are separated by 30 days. Adapted from Borogovac et al. <sup>111</sup>

Within-session data clearly demonstrated the expected activation in the occipital lobe and the primary motor cortex and supplementary motor cortex (Figure 1.6, left panel). However, when rest and task data were separated by 30 days, significant voxels unrelated to the task were observed (Figure 1.6, right panel). In particular, the magnitude and extent of activation in the motor regions and occipital lobe have increased and spurious activation is detected. As previously discussed, between-session variability is dominated by physiological sources of error. Therefore, it is highly possible that the observed spurious activation is caused by between-session repositioning errors and the increased magnitude and extent of activation is related to fluctuations in basal blood flow between sessions. These sources of error are detrimental for longitudinal studies, as false positive activation could be misinterpreted as activation related to physiology. By taking these

sources of variation into account, the aim of my thesis is to investigate whether ASL has the sensitivity to detect longitudinal changes in CBF within an individual at the voxel-wise level.

## Chapter 2

### 2 Methods

#### 2.1 Study Design

The purpose of this study was to investigate the ability of ASL to detect long-term changes in brain function through the associated changes in regional CBF. By accounting for sources of variance that can have a significant impact on longitudinal monitoring, the aim was to show that ASL has the sensitivity to detect activation-induced changes in regional CBF over periods extending up to a month despite its relatively poor spatial resolution ( $4 \times 4 \times 6 \text{ mm}^3$ ). Previous studies have demonstrated low variability in resting CBF and the ability of ASL to detect activation between imaging data acquired on separate days<sup>34,102,109,111</sup>. However, most of these studies relied on ROI-based analysis rather than the voxel-wise as would be performed on data collected in the same imaging session. This work extends on these studies by investigating voxel-wise reproducibility, reliability and the precision of activation maps produced when resting data were separated from task data by periods up to a month.

To assess the ability of ASL to detect longitudinal activation, a simple finger tapping task was chosen because it is a well-studied paradigm that produces focal and robust activation in the sensorimotor network<sup>112</sup>. These characteristics are advantageous for assessing the quality of activation maps generated from data acquired on separate days because it is relatively straightforward to distinguish between true activation and false positives based on the well-defined activation patterns associated with motor tasks. To replicate a potential longitudinal study design that could be used in a clinical cohort, for instance to assess treatment response in chronic-pain patients, data were collected in three imaging sessions separated by a week and a month.

### 2.1.1 Activation Paradigm

In each of the three imaging sessions, ASL images were acquired continuously (see Section 1.3.1 for details) during a 5-min rest period followed by a 5-min period of self-paced sequential finger tapping (right-hand). Volunteers were instructed to lay still with their eyes closed during the rest period and not focus on a particular task.



**Figure 2.1:** Sequence for sequential finger tapping; (1) thumb to index finger, (2) thumb to middle finger, (3) thumb to ring finger, (4) thumb to little finger, (5) thumb to ring finger, (6) thumb to middle finger, and (7) restarting the sequence from the beginning.

To start the task period, volunteers were verbally cued to begin briskly tapping the tip of their thumb to each finger with their right hand in a sequential manner, starting with the index finger and ending on the little, followed by a repetition of the task in reverse (Figure 2.1).

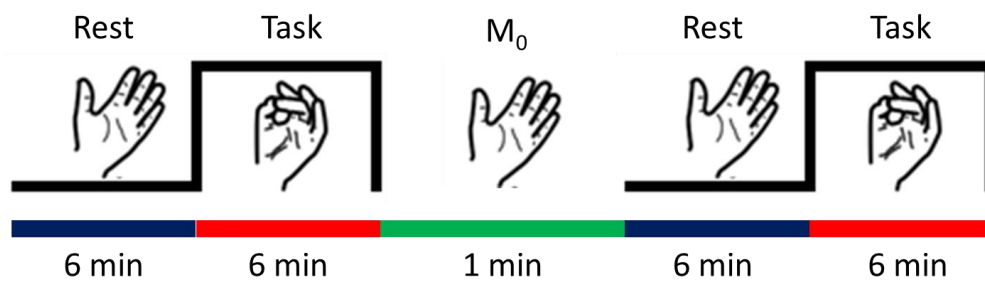


**Figure 2.2:** Schematic of motor task paradigm. During the ASL sequence, volunteers perform a rest and finger tapping task twice. Each epoch lasted 5:36 min (approximately 6 min). Between the two runs, the equilibrium image (M<sub>0</sub>) is acquired.

This sequence was repeated throughout the task period. The entire rest-task paradigm was performed twice within each imaging sessions with a short delay (~ 1 min) between runs (Figure 2.2). Volunteers were monitored from the control room of the MRI suite to ensure the task was being performed properly.

Dividing the rest and task data into two distinct periods, rather than using a more traditional block design consisted of shorter epochs (e.g. 30 s), was chosen in order to combine rest and task CBF data from different imaging sessions. That is, baseline CBF reproducibility and reliability was assessed: (1) within session by comparing CBF images from the two rest periods, and (2) between sessions by comparing the rest CBF images from the first session to its counterpart from the second session (1 week separation) and the third session (1 month separation). In a similar fashion, activation maps associated with finger tapping were generated from within-session and between-session analysis. Within-session activation maps were obtained using rest and task CBF images from the same run within a session. Between-session maps were generated using the task CBF images from session 1, and either the rest CBF images from the second (1 week separation), or the third session (1 month separation). For the between-session analysis, the task data always remained the same (i.e. from session 1) and, therefore, any deviations in the activation maps would be caused by either fluctuations in resting CBF across days or registration errors when aligning images from separate sessions. Activation data from runs 1 and 2 were concatenated separately; task data from run 1 was always compared to baseline data from run 1 (and similarly for run 2), to avoid confounding effects, such decreased attentional processing between runs<sup>82</sup>. Provided that sources of between-session variation, such as repositioning errors are minimal, variability in baseline CBF should be similar to the within-session variation. Likewise, the between and within-session activation maps should be similar.

### 2.1.2 Arterial Transit Time Imaging

Signal changes caused by variations in ATTs can be a significant confounder to ASL perfusion measurements. Accurate quantification of CBF when using an ASL protocol with a single PLD relies on the assumption that the labeled arterial blood water will reach the imaging slice and exchange with tissue water prior to image acquisition, which may not always occur. In addition, variations in ATT across days could reduce the reproducibility of the CBF images. Therefore, a second goal of this study was to acquire ATT images in each of the three imaging sessions in order to determine the between-session variability in ATT.

A challenge with measuring ATTs is it requires acquiring ASL images at multiple PLDs, which can significantly increase the overall acquisition time (up to 25 minutes)<sup>69</sup>. For this reason, ATT imaging is not routinely performed<sup>111</sup>. One approach for reducing the imaging time, which was adapted in this study, is to collect ASL images used to map ATT at a lower spatial resolution since variations in ATTs tend to occur between large vascular territories<sup>69</sup>. Lowering the image resolution (e.g. from 3 x 3 x 5 mm<sup>3</sup> to 12 x 12 x 4 mm<sup>3</sup>) improves voxel-based SNR, thereby reducing the number of acquisitions required to map ATT.

## 2.2 Volunteers

The study was approved by University Research Ethics Board and all volunteers provided written informed consent prior to each session. Seven healthy right-handed volunteers (2 male, 5 female, aged  $22.6 \pm 1.3$  years) participated in the study.



## 2.3 Between-Session Variability

Subjects were instructed to get adequate sleep and abstain from consuming coffee and food for at least 6 hours and alcohol for 24 hours prior to scanning due to their potential vasomotor effects on CBF<sup>113</sup>. The majority of scans were scheduled in the morning to minimize the effect of diurnal CBF fluctuations<sup>85</sup>.

An immobilizing head mold was used to restrict motion within a session and to reduce variability in head position between sessions. The polyurethane foaming agent was formed by the reaction of methylene diphenyl diisocyanate (MDI) with a polyol (Alpha Cradle, Smithers Medical Products, Inc.). The foaming agent was poured into a bag and which was placed under the volunteer's head inside the head coil. Anatomical landmarks (nose and eyebrows) were aligned to location markers on the head coil using the external laser positioning system (LAP Laser, Lüneburg, Germany). Subjects were required to remain still while the mold set (approximately 15 minutes). On return visits, each subject's individual head mold was reused in order that the position of their head from the first session could be reproduced as closely as possible.

As a secondary step to further minimize errors due to image misalignments, manual alignment was performed based on comparing structural MRIs acquired in the first and subsequent session. First, using a sagittal structural image, the anterior-to-posterior commissure angle was compared to that measured in the first session and a 0 - 6° adjustment in the angle of the slice was made to reproduce the same slice positioning. Second, using the axial structural image, slice positioning in the head to foot direction was adjusted to match the slice location on the first day by comparing easily identifiable landmarks (i.e. eyes, skull and acoustic nerves). Typically, the axial slice positioning was adjusted by 0 - 2.5 mm to improve the alignment relative to the images acquired in the

first session. Following these adjustments, a second axial structural MRI image was acquired to confirm the accuracy of the axial positioning.

## 2.4 Data Acquisition

All imaging was conducted using a Siemens 3 T Biograph mMR scanner equipped with a 32-channel head coil (Siemens Medical Systems, Erlangen, Germany). Imaging sessions began with a localizer scan, followed by the acquisition of high-resolution sagittal T1-weighted magnetization prepared rapid gradient echo (MPRAGE) image (repetition time (TR)/echo time (TE): 2000/2.98 ms, flip angle: 9°, field of view (FOV): 256 x 256 mm<sup>2</sup>, 176 slices, voxel size: 1 mm<sup>3</sup> isotropic resolution, scan duration: 3:35 min). This imaging volume was used for sagittal manual image alignment, spatial normalization of the ASL images to Montreal Neurological Institute (MNI) co-ordinates and to generate grey and white matter fractional tissue maps. Axial turbo spin echo (TSE) T2-weighted images (TR/TE: 6100/106 ms, flip angle: 120°, FOV: 220 x 220 mm<sup>2</sup>, 31 slices, voxel size: 0.57 x 0.57 x 4 mm<sup>3</sup>, gap: 0.8 mm, scan duration =2:14 min) were acquired for the previously described axial manual online image realignment.

ASL images were acquired using single-shot 3D gradient/spin-echo (GRASE) sequence with the following parameters: TR/TE: 3500/22.76 ms, label duration: 1500 ms, PLD: 1200 ms, FOV: 240 x 240 mm<sup>2</sup>, 24 axial slices, voxel size = 3.8 x 3.8 x 6 mm<sup>3</sup>, scan time = 11:12 min)<sup>114</sup>. A pseudo continuous labeling scheme was applied 90 mm below the center slice. As described in section 2.1.1, the pCASL sequence was performed twice for the two finger tapping runs. Each run, a total of 96 control-tag pairs were acquired for the rest and task period (48 control-tag pairs for each condition). Between the runs, an image set of the equilibrium magnetization was acquired with the same GRASE sequence: TR/TE: 5000/22.76 ms, PLD: 4000 ms and scan time: 30s.

For ATT mapping, ASL images were acquired at five PLDs: 700, 1300, 1900, 2500 and 3100 ms. The other changes to the sequence included 5 control/tag images per PLD, TR/TE: 6000/18.76 ms, FOV: 500 x 500 mm<sup>2</sup>, voxel size: 12 x 8 x 6 mm<sup>3</sup>, and a total scan time of 5 min.

## 2.5 Image Processing and Analysis

### 2.5.1 Perfusion-Weighted Imaging

Data was first converted from Digital Imaging and Communications in Medicine (DICOM) format to Neuroimaging Informatics Technology Initiative (NIfTI) format. Images were checked for gross motion: translations greater than 3 mm and rotations greater than 3° as defined by Wang et al. <sup>115</sup>. Image processing was performed with SPM8 (Wellcome Trust Center for Neuroimaging, University College London, UK), FSL (FMRIB Software Library, Functional Magnetic Resonance Imaging of the Brain Centre, University of Oxford, Oxford, UK) and MATLAB (2012a, The MathWorks, Natick, MA). The main pre-processing steps are summarized in Figure 2.3. Raw pCASL and M0 data from all sessions were realigned to the first image using a least squares approach and a six-parameter rigid body spatial transformation. In this step, the first scan of sessions 2 and 3 were aligned to the first scan of session 1. Next, the remaining scans within each session were aligned to the newly aligned first scan of the session (individually). Together, these steps corrected for possible differences in head positioning between sessions and within-session motion. Raw ASL data were pair-wise subtracted to generate  $\Delta M$  images. Pairwise subtraction of control and label images was performed using ASLtbx <sup>115</sup>. T1-weighted images were skull stripped using FSL brain extraction tool (BET) to improve the co-registration and segmentation process <sup>116</sup>. Skull-stripped T1-weighted images were then segmented using unified segmentation. This step served two purposes: First, to generate a grey matter mask used to estimate of grey matter CBF; and

second, to generate normalization parameters based on morphology of the brain <sup>117</sup>. Each subject's M0 image was co-registered to their respective skull-stripped high-resolution T1-weighted image with a rigid body transformation to correct for in-plane shifts and rotations and to improve the accuracy of the normalization process.

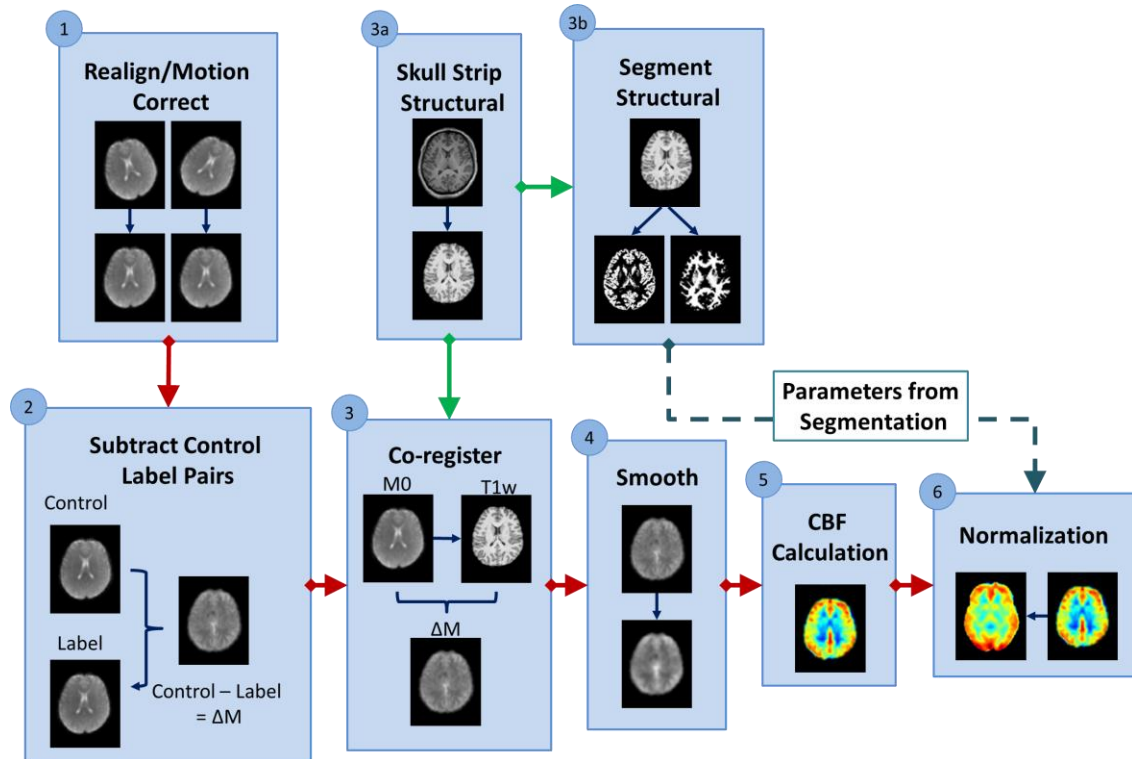


**Figure 2.3:** Overview of preprocessing steps. Green arrows represent the structural processing pipeline and red arrows represent perfusion weighted image pipeline. Briefly, (1) images were motion corrected; (2) ASL images were pairwise subtracted; T1-weighted images were skull stripped (3a) and segmented into grey matter and white matter (3b); (3) M0 images were co-registered to skull stripped T1-weighted images (from step 3a) and the parameters were applied to the  $\Delta M$  images; (4)  $\Delta M$  and M0 images were smoothed; (5) CBF was calculated and (6) spatially normalized by applying normalization parameters from the segmentation step.

Transformations were estimated iteratively by minimizing the cost function representing the sum of squares difference in intensities between the anatomical and functional image. Parameters required to transform the M0 image were applied to the time series of  $\Delta M$

images. The resulting  $\Delta M$  images were then smoothed with an isotropic 6 mm full width at half maximum (FWHM) Gaussian kernel to improve the SNR and eliminate any remaining anatomical variability. ASL images were converted into physiological units (mL/100g/min) using a single compartment flow model (Equation (2.1))<sup>118</sup>.

$$f = \frac{\Delta M \lambda e^{\frac{\omega}{T_{1a}}}}{2\alpha M_0 T_{1a} \left(1 - e^{\frac{-(\tau + \omega)}{T_{1a}}}\right)} \quad (2.1)$$

The following assumptions were made:  $\lambda$  = blood/tissue water partition coefficient, 0.9 g/mL<sup>71</sup>;  $\alpha$  = labeling efficiency 86%<sup>69</sup>;  $\omega$  = post-labeling delay of 1.2 s;  $\tau$  = label duration 1.5 s; and  $T_{1a} = 1.650$  s<sup>119</sup>. Deformation parameters generated in the segmentation step were used to transform CBF maps into MNI space.

## 2.5.2 Arterial Transit Time Images

All raw ASL data were realigned using the same two-step process as the single PLD ASL data. Using ASLtbx, control images were subtracted from their labeled pair. The FSL BET routine was used to skull strip both the T1-weighted and ATT images. A voxel-wise parametric fit of perfusion-weighted data to the one compartment kinetic model was performed using the fast ASL and BOLD Bayesian estimation routine (FSL, FABBER)<sup>120</sup>. The Bayesian approach provides more robust estimates of ATT and CBF using prior knowledge about the parameters (i.e. CBF, ATT, bolus length, T1 of tissue) based on biophysically realistic assumptions<sup>121</sup>. The model included spatial priors and was iterated 200 times to maximize convergence. The resulting estimate of ATT was co-registered to their respective T1-weighted image volume using a rigid-body transformation in SPM. Next, skull stripped T1-weighted and ATT images were normalized to the MNI template using the SPM T1-weighted template.

## 2.6 Reproducibility of Arterial Spin Labeling

### 2.6.1 Variability in Resting Cerebral Blood Flow

Using a 2 x 3 (2 runs / 3 sessions) voxel-wise repeated measures ANOVA that was implemented in MATLAB, variance was decomposed into within and between-session contributions, which were used to calculate reproducibility and reliability. Reproducibility was measured using the wsCV<sup>122</sup> given by:

$$wsCV = \frac{SD_{\Delta CBF}}{Mean_{CBF}} \cdot 100 \quad (2.2)$$

where  $SD_{\Delta CBF}$  represents the standard deviation of CBF between repeated measurements (i.e. for within-session,  $SD_{\Delta CBF}$  represents the standard deviation between runs, and for between-session, it represents the standard deviation between sessions).  $Mean_{CBF}$  is the average CBF across all sessions. Reliability was measured using a two way mixed model ICC of absolute agreement<sup>77</sup>. This is given by:

$$ICC = \frac{\sigma_{bs}^2}{\sigma_{bs}^2 + \sigma_{se}^2 + \sigma_{er}^2} \quad (2.3)$$

where  $\sigma_{bs}^2$  is the between subject variance,  $\sigma_{se}^2$  is the systemic error (variance between the repeated measures), and  $\sigma_{er}^2$  is the error variance. For the within-session ICC,  $\sigma_{se}^2$  represents the variability between runs, and for the between-session ICC,  $\sigma_{se}^2$  represents the variability between sessions. Reliability and reproducibility were also assessed within regions of interests (ROIs): two based on tissue type (grey and white matter), the four major lobes (frontal, parietal, temporal, occipital lobe) and pain regions (anterior cingulate cortex, amygdala, hippocampus, insular cortex, posterior cingulate cortex, somatosensory cortex and thalamus). Lobe and pain region ROIs were defined using the Automated Anatomical Labeling (AAL) atlas within the wfupickatlas toolbox in SPM8.

Grey and white matter masks were generated by thresholding the corresponding SPM8 probability maps by 80 and 60% respectively. Measurements of reliability and reproducibility within ROIs were generated by multiplying ICC and wsCV images by dichotomous masks and averaging the values within the defined region.

A 2 x 3 repeated measures ANOVA was conducted with IBM SPSS Statistics (Version 20.0, IBM Corp, Armonk, NY) to test for differences in resting CBF across sessions and between lobes and tissue types. To assess the effect of day-to-day variations in baseline CBF on the reproducibility and reliability of CBF, voxel-wise analysis of resting CBF was performed using absolute CBF (aCBF) and CBF intensity normalized by mean grey matter CBF (i.e. relative CBF, rCBF).

### 2.6.2 Variability in Arterial Transit Time

A group mean ATT map was calculated for each session to visualize regional variability. Reproducibility of ATT was assessed at the voxel-wise level and within grey matter. For each voxel, wsCV between subjects and between sessions was calculated using variance derived from the repeated measures ANOVA implemented in MATLAB. In addition, using SPM, a contrast comparing ATT across sessions (within-subjects repeated measures design) was formulated to test for significant voxel-wise differences. Since ATT patterns across the brain are dependent on which vessel they are being supplied by, namely the anterior cerebral artery (ACA), middle cerebral artery (MCA) or posterior cerebral arteries (PCA), reproducibility was assessed within these regions. ROIs of the vascular territories were defined using the AAL template in wfupickatlas based on templates established by Tatu et. al<sup>123</sup>. A 1 x 3 (1 run x 3 sessions) repeated measures ANOVA was used to test for differences in ATT between sessions and between vascular territories in SPSS.

## 2.6.3 Motor Activation

### 2.6.3.1 Reliability and Reproducibility

Activation maps were generated at the subject level for each contrast. Contrasts were generated by concatenating task data from the first session with rest data from: (a) the same session, (b) the second session at 1 week and (c) the third session at 1 month as shown in Figure 2.4.

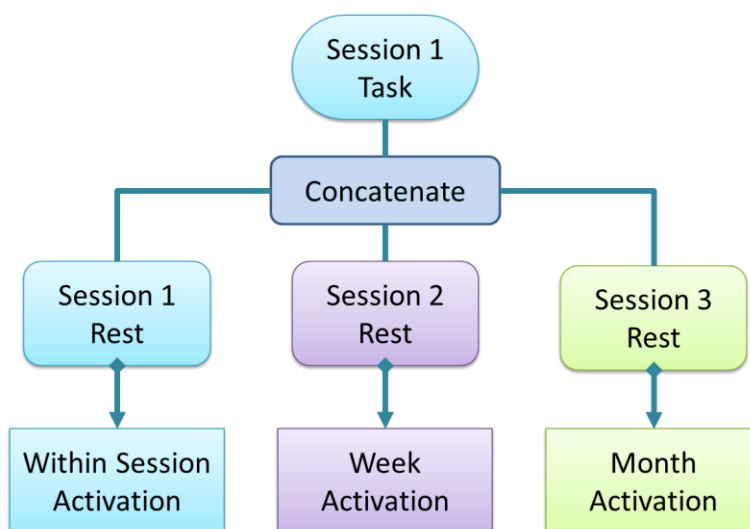


**Figure 2.4:** Schematic describing the formation of activation contrasts based on within-session data and between-session data (1 week and 1 month). Notice that for each of the contrasts, the task remains the same, while the rest period changes.

Analyses were performed using aCBF and rCBF data sets. Since normalizing by the grey matter CBF has no effect on within-session activation (i.e., both rest and task data sets are scaled by the same intensity), only aCBF activation maps were generated for the within-session analysis. Thus, a total of 5 contrasts were generated for each subject. The first image set of each series was removed to as the magnetization was not at equilibrium. It is important to emphasize that the task data remained the same for all contrasts, while the



rest data varied based on which imaging session it was obtained. Activation maps were generated using the standard first level GLM analysis in SPM8. Areas of activation were identified with the  $t$  statistic after correction for multiple comparisons using the family wise error rate (FWE) ( $p < .05$ ) and no cluster size threshold.

### 2.6.3.2 Precision of Motor Task Activation

Precision was used to assess the number of false positives detected within session compared to when rest and task were separated by either a week or a month. Significant within-session activation, as detected by GLM analysis, was used as the ground truth. To avoid bias, activated regions from run 2 data were used as the ground truth for the run 1 analysis and vice versa. In addition, masks were dilated by 3 voxels isotropically to include additional voxels related to motor activation. Voxels were classified as a TP or FP based on their state (activated or not activated) relative to ground truth.

## Chapter 3

### 3 Results

#### 3.1 Study Demographics

Five female and two male right-handed volunteers aged  $22.6 \pm 1.3$  years participated in the study. Subjects were scanned during 3 sessions separated by a week ( $7.0 \pm 0.5$  days) and a month ( $28.9 \pm 2.5$  days). Task data from the first run of the first session for subject 1 was removed from the analysis because the task was not performed correctly. A summary of scan times for each subject is displayed in Table 3.1. While the majority of the scans took place in the morning, 5 of 21 scans took place in the afternoon due to scheduling conflicts.

**Table 3.1:** Scan times for each subject. Scans taken in the afternoon are shown in bold.

Subject	Session 1	Session 2	Session 3
1	9am	<b>4pm</b>	9am
2	9am	<b>2pm</b>	<b>1pm</b>
3	9am	<b>2pm</b>	9am
4	9am	9am	9am
5	9am	9am	9am
6	<b>1pm</b>	9am	9am
7	7am	8am	9am

#### 3.2 Alignment of Images

Figure 3.1 shows T2-weighted images of a representative subject acquired during three sessions separated by a week and a month (relative to the first session). No additional post processing steps were applied to these images. Notice the good alignment of the images from the second and third session relative to the image from the first session, despite the separation in time. Within-session motion was characterized in terms of the

rigid transformation (translation and rotation) between the first image of the first run relative to the first image of the second run required to align images in the realignment step. Similarly, between-session motion was defined as the difference in translation between the first images from the two separate sessions (i.e. the first session and either the second or third session).

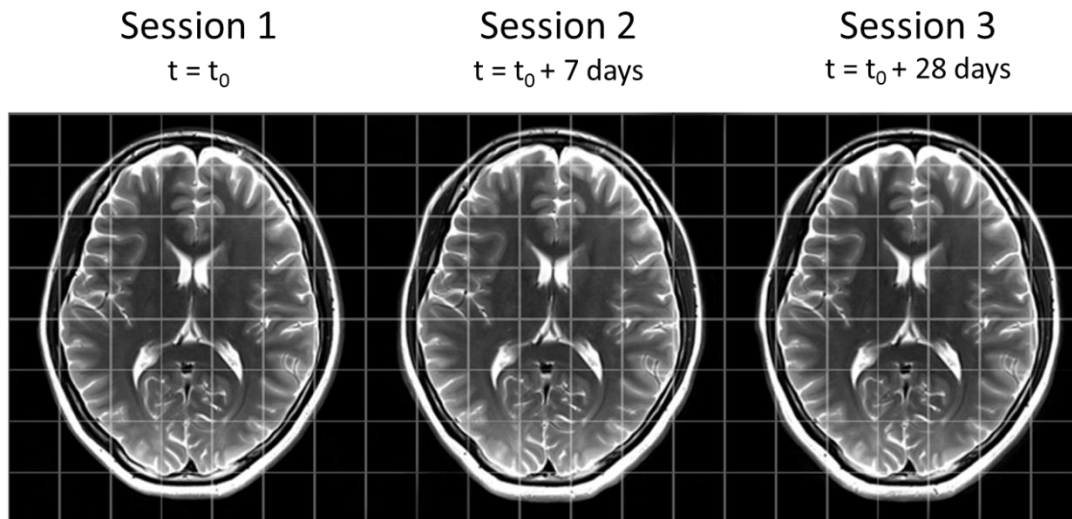


**Figure 3.1:** T2-weighted images acquired during three imaging sessions. Despite the separation in time and absence of post processing steps (i.e. realignment), the images are near identical. For this particular subject, the between-session parameters required to align images were:  $0.06 \pm 0.02$ ,  $1.26 \pm 0.62$  and  $0.43 \pm 0.55$  mm translations in the x, y, and z direction respectively and  $0.36 \pm 0.25$ ,  $0.09 \pm 0.02$  and  $0.02 \pm 0.02^\circ$  rotations in the pitch roll and yaw direction, respectively.

Averaged rotation (roll, pitch, yaw) and translation (x, y, z) parameters from the realignment step within- and between-sessions are shown in Table 3.2. Transformations required to align images within the same session were similar to those when aligning images from two separate sessions. No significant differences were found between the within-session and between-session translation parameters; although, the magnitude of the latter was generally higher.

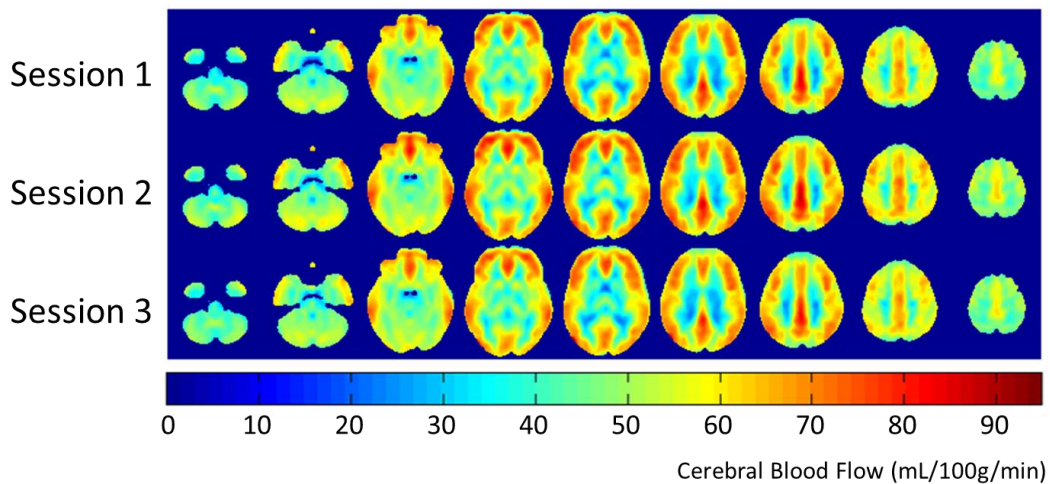
**Table 3.2:** Mean translation and rotation parameters within and between sessions.

	Translation (mm)			Rotation (degrees)		
	x	y	z	pitch	roll	yaw
<b>Within Session</b>	0.30 ± 0.50	1.48 ± 0.37	0.46 ± 0.66	0.22 ± 0.08	0.14 ± 0.10	0.09 ± 0.08
<b>Between Sessions</b>	0.45 ± 0.76	0.97 ± 0.19	0.67 ± 0.71	0.36 ± 0.38	0.23 ± 0.26	0.14 ± 0.28

### 3.3 Analysis of Resting Cerebral Blood Flow

#### 3.3.1 Mean Resting Blood Flow

Figure 3.2 shows group averaged mean resting aCBF maps for each session. Within grey matter the mean CBF was  $55.9 \pm 9.05$ ,  $58.2 \pm 4.9$ ,  $56.0 \pm 5.8$  mL/100g/min for sessions 1, 2 and 3 respectively.

**Figure 3.2:** MNI normalized group average mean resting CBF in ml/100g/ml for sessions 1, 2 and 3. (N=7)

Using the FWE rate ( $p < .05$ ), voxel-wise within-subjects repeated measures ANOVA revealed no significant differences resting absolute or relative CBF across sessions or

between runs. Table 3.3 summarizes mean CBF across subjects within each ROI for each session and run. Mean CBF demonstrates consistent flow over time. Differences in CBF within session (run 1 vs run 2) and between sessions (session 1 vs session 2 vs session 3) were not significant for any of the ROIs. Since there was no significant main effect of session on CBF, pairwise comparisons between individual sessions were not assessed. There was also no significant difference in CBF between the 4 major lobes; however, white matter CBF was significantly lower than grey matter CBF ( $p < .05$ ).

**Table 3.3:** Mean resting CBF (ml/100g/ml) in select ROIs (N = 7). ( $\pm$  standard deviation)

ROI	Session 1		Session 2		Session 3	
	Run 1	Run 2	Run 1	Run 2	Run 1	Run 2
<i>Tissue Class</i>						
Grey Matter	57.0 $\pm$ 8.8	54.8 $\pm$ 9.3	59.3 $\pm$ 5.0	57.0 $\pm$ 4.8	56.0 $\pm$ 5.5	55.9 $\pm$ 6.1
White Matter	45.1 $\pm$ 7.6	43.7 $\pm$ 6.7	47.9 $\pm$ 2.9	45.3 $\pm$ 2.6	44.8 $\pm$ 5.1	44.8 $\pm$ 4.6
<i>Lobes</i>						
Frontal Lobe	57.2 $\pm$ 9.7	54.7 $\pm$ 9.6	59.4 $\pm$ 5.7	57.4 $\pm$ 4.7	56.2 $\pm$ 5.5	56.0 $\pm$ 5.7
Temporal Lobe	57.0 $\pm$ 8.5	54.6 $\pm$ 8.5	59.5 $\pm$ 4.7	56.4 $\pm$ 3.9	56.1 $\pm$ 5.6	55.7 $\pm$ 5.2
Occipital Lobe	56.8 $\pm$ 9.7	55.6 $\pm$ 10.0	59.8 $\pm$ 8.2	56.7 $\pm$ 6.6	56.6 $\pm$ 9.6	56.9 $\pm$ 9.0
Parietal Lobe	56.5 $\pm$ 10.4	54.4 $\pm$ 9.6	58.6 $\pm$ 5.4	56.2 $\pm$ 4.3	55.3 $\pm$ 6.5	55.5 $\pm$ 6.5
<i>Pain Regions</i>						
Anterior Cingulate	60.4 $\pm$ 8.9	57.2 $\pm$ 9.9	62.9 $\pm$ 5.6	60.3 $\pm$ 5.2	59.6 $\pm$ 5.3	59.2 $\pm$ 6.0
Amygdala	42.1 $\pm$ 5.3	41.0 $\pm$ 5.7	46.1 $\pm$ 4.5	43.8 $\pm$ 3.9	42.3 $\pm$ 3.4	42.8 $\pm$ 4.4
Hippocampus	43.2 $\pm$ 5.0	42.1 $\pm$ 6.6	46.1 $\pm$ 3.9	44.5 $\pm$ 3.4	43.3 $\pm$ 4.0	44.1 $\pm$ 4.3
Posterior Cingulate	55.0 $\pm$ 8.1	52.6 $\pm$ 7.0	56.7 $\pm$ 4.2	54.9 $\pm$ 2.5	54.7 $\pm$ 5.1	54.6 $\pm$ 5.0
Somatosensory Cortex	52.5 $\pm$ 6.6	52.8 $\pm$ 5.9	57.8 $\pm$ 4.2	53.2 $\pm$ 3.1	51.7 $\pm$ 5.0	52.3 $\pm$ 4.0
Insular Cortex	51.8 $\pm$ 9.1	49.7 $\pm$ 8.1	54.3 $\pm$ 5.5	52.1 $\pm$ 4.0	51.2 $\pm$ 5.8	51.3 $\pm$ 6.2
Thalamus	42.7 $\pm$ 8.2	46.0 $\pm$ 6.0	50.4 $\pm$ 3.9	44.8 $\pm$ 4.4	40.3 $\pm$ 7.3	44.4 $\pm$ 7.4

### 3.3.2 Reproducibility of Resting Blood Flow

WsCV maps assessing variability in resting CBF within- and between-sessions are shown in Figure 3.3. The histogram represents the frequency distribution of voxel-wise wsCV values for within and between-session analysis. Results are presented for error analysis of absolute and relative CBF.

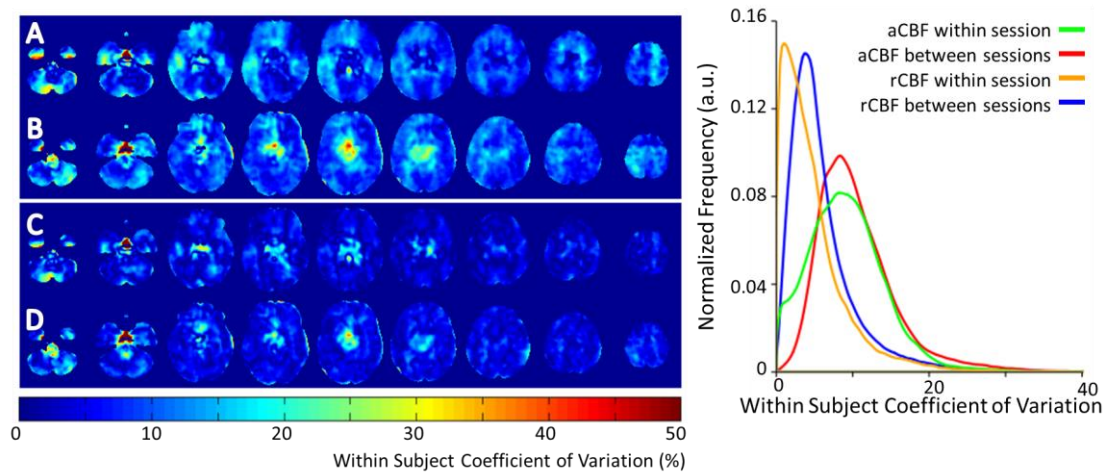


**Figure 3.3:** Relative and absolute voxel-wise wsCV maps for: (A) within-session aCBF images (B) between-sessions aCBF images (C) within-session rCBF images, and (D) between-session rCBF images. The corresponding histograms to the right display the distributions of voxel-wise within- and between-sessions wsCV values for both aCBF and rCBF data sets.

All wsCV maps were relatively homogeneous throughout cortical grey matter. The corresponding mean wsCV values for aCBF were  $9.1 \pm 5.2\%$  and  $10.0 \pm 4.9\%$  for the within-session and between-session analyses. Using the rCBF images, within-session wsCV reduced to  $4.7 \pm 4.5\%$  and between-session wsCV reduced to  $5.7 \pm 4.5\%$ . It is evident from visual inspection of the wsCV maps that there was a global increase in wsCV in the aCBF images compared to the rCBF images. This increased variance for aCBF is reflected by its broader and right-shifted distribution in the histograms for both the within-session and between-session results, and confirmed by the ROI analysis (Table 3.4). Average wsCV values in the majority of ROIs for both within and between-session results were higher for aCBF compared to rCBF.

**Table 3.4:** Mean voxel-wise wsCV for absolute and relative resting CBF in select ROIs ( $\pm$  standard deviation).

ROI	aCBF wsCV (%)		rCBF wsCV(%)	
	Within Session	Between Session	Within Session	Between Session
<i>Tissue Class</i>				
Grey Matter	9.1 $\pm$ 5.2	10.0 $\pm$ 4.9	4.7 $\pm$ 4.5	5.7 $\pm$ 4.4
White Matter	9.8 $\pm$ 4.6	10.9 $\pm$ 4.7	4.4 $\pm$ 4.0	5.6 $\pm$ 3.4
<i>Lobes</i>				
Frontal Lobe	9.1 $\pm$ 4.1	10.0 $\pm$ 4.0	3.6 $\pm$ 2.8	5.1 $\pm$ 3.1
Temporal Lobe	7.8 $\pm$ 4.0	8.1 $\pm$ 3.0	4.0 $\pm$ 3.0	4.8 $\pm$ 2.8
Occipital Lobe	8.7 $\pm$ 3.6	8.9 $\pm$ 3.6	3.0 $\pm$ 2.3	5.1 $\pm$ 3.1
Parietal Lobe	11.5 $\pm$ 5.5	9.2 $\pm$ 3.7	4.9 $\pm$ 3.8	4.8 $\pm$ 3.6
<i>Pain Regions</i>				
Anterior Cingulate	11.2 $\pm$ 2.8	9.8 $\pm$ 3.5	3.1 $\pm$ 1.8	4.4 $\pm$ 2.3
Amygdala	8.6 $\pm$ 3.4	15.9 $\pm$ 4.3	4.2 $\pm$ 5.0	7.8 $\pm$ 3.3
Hippocampus	8.0 $\pm$ 4.8	12.3 $\pm$ 4.5	6.9 $\pm$ 6.5	6.5 $\pm$ 4.1
Posterior Cingulate	8.3 $\pm$ 5.0	13.6 $\pm$ 4.5	5.8 $\pm$ 5.7	6.2 $\pm$ 4.1
Somatosensory Cortex	9.2 $\pm$ 4.1	10.2 $\pm$ 4.2	3.5 $\pm$ 2.8	5.4 $\pm$ 3.5
Insular Cortex	8.7 $\pm$ 4.1	7.7 $\pm$ 2.8	3.5 $\pm$ 2.4	5.0 $\pm$ 2.4
Thalamus	5.1 $\pm$ 3.6	21.7 $\pm$ 8.1	13.4 $\pm$ 5.5	14.6 $\pm$ 7.3

While aCBF and rCBF within most ROIs had good reproducibility (wsCV < 20%), wsCV was noticeably higher in midbrain regions for the between-session analysis (Figure 3.3 B &D), particularly for the aCBF images. For example, the mean wsCV in the thalamus was 21.7  $\pm$  8.1% for between-session analysis of aCBF images. This increased variance was reduced by global normalization – in the thalamus the between-session wsCV reduced to 14.6% in the rCBF images, but this value is still higher than corresponding cortical and subcortical regions.

### 3.3.3 Reliability of Resting Blood Flow

ICC maps and their corresponding histograms are displayed in Figure 3.4. The histogram distribution represents the frequencies of voxel-wise ICC values from the within and between-session analysis. Results are presented for both absolute and relative CBF.

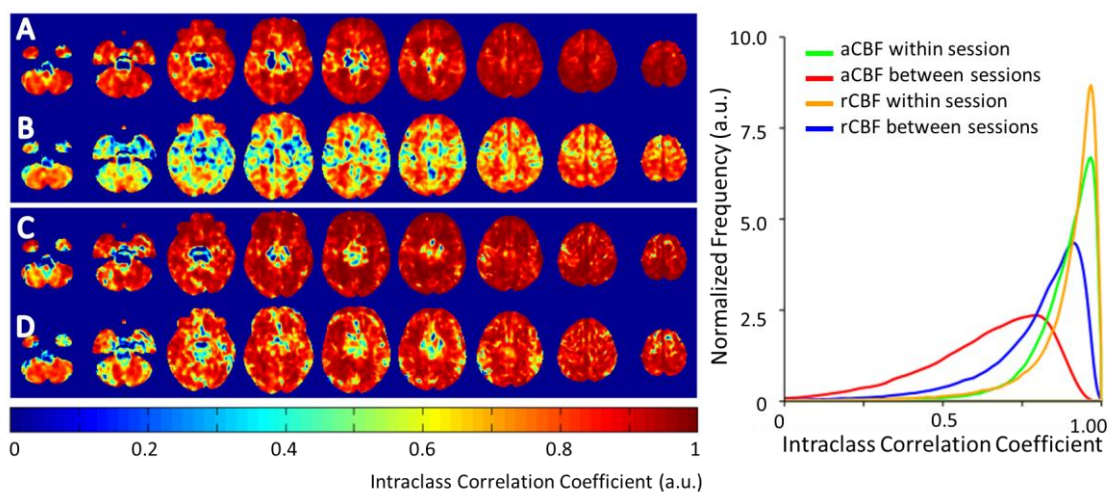


**Figure 3.4:** Voxel-wise ICC maps within and between sessions calculated using absolute CBF and CBF scaled by mean grey matter CBF (rCBF). (A) within-session aCBF (B) between-sessions aCBF (C) within-session rCBF and (D) between-session rCBF. Corresponding histogram displaying frequency of ICC values in voxel-wise maps is displayed to the right.

The ICC maps depict excellent within-session grey matter reliability, with ICC values consistently above 0.75. This is also shown in the corresponding histograms in Figure 3.4: the distributions of ICC values for within-session reliability, shown in orange and green, are skewed towards a maximum value of 1. Average within-session grey matter ICC for the aCBF images was  $0.85 \pm 0.23$  and  $0.89 \pm 0.20$  for the rCBF images. Average within-session and between-session ICC values for all ROIs are given in Table 3.5. Similar to the wsCV results, mean voxel-wise ICC values was greater within session compared to between-sessions and for rCBF images compared to aCBF images. Within



grey matter, between-session reliability calculated with aCBF was good ( $0.66 \pm 0.19$ ) while rCBF reliability was excellent ( $0.84 \pm 0.15$ ).

**Table 3.5:** Mean voxel-wise ICC for absolute and relative resting CBF in select ROIs ( $\pm$  standard deviation).

ROI	aCBF ICC		rCBF ICC	
	Within Session	Between Session	Within Session	Between Session
<i>Tissue Class</i>				
Grey Matter	$0.85 \pm 0.23$	$0.66 \pm 0.19$	$0.89 \pm 0.20$	$0.84 \pm 0.15$
White Matter	$0.87 \pm 0.17$	$0.69 \pm 0.17$	$0.92 \pm 0.13$	$0.86 \pm 0.12$
<i>Lobes</i>				
Frontal Lobe	$0.93 \pm 0.06$	$0.71 \pm 0.16$	$0.93 \pm 0.07$	$0.85 \pm 0.13$
Temporal Lobe	$0.91 \pm 0.06$	$0.72 \pm 0.12$	$0.92 \pm 0.07$	$0.85 \pm 0.11$
Occipital Lobe	$0.94 \pm 0.05$	$0.75 \pm 0.14$	$0.93 \pm 0.07$	$0.85 \pm 0.12$
Parietal Lobe	$0.86 \pm 0.11$	$0.54 \pm 0.21$	$0.90 \pm 0.1$	$0.79 \pm 0.17$
<i>Pain Regions</i>				
Anterior Cingulate	$0.90 \pm 0.06$	$0.66 \pm 0.14$	$0.95 \pm 0.04$	$0.84 \pm 0.11$
Amygdala	$0.70 \pm 0.27$	$0.34 \pm 0.17$	$0.72 \pm 0.28$	$0.64 \pm 0.19$
Hippocampus	$0.68 \pm 0.28$	$0.45 \pm 0.18$	$0.68 \pm 0.32$	$0.73 \pm 0.2$
Posterior Cingulate	$0.78 \pm 0.24$	$0.61 \pm 0.2$	$0.87 \pm 0.16$	$0.83 \pm 0.13$
Somatosensory Cortex	$0.94 \pm 0.06$	$0.74 \pm 0.16$	$0.91 \pm 0.08$	$0.87 \pm 0.09$
Insular Cortex	$0.88 \pm 0.08$	$0.55 \pm 0.21$	$0.92 \pm 0.07$	$0.84 \pm 0.10$
Thalamus	$0.44 \pm 0.39$	$0.55 \pm 0.21$	$0.61 \pm 0.21$	$0.68 \pm 0.17$

### 3.4 Arterial Transit Time Reproducibility

Mean grey matter ATT values averaged across subjects were  $806 \pm 45$ ,  $801 \pm 35$ , and  $796 \pm 39$  ms for sessions 1, 2 and 3, respectively. There were no significant differences between values. Group mean ATT maps for each of the three sessions are shown in Figure 3.5. Regional heterogeneity in ATTs was observed, with increased ATT towards medial posterior and medial frontal regions of the brain.

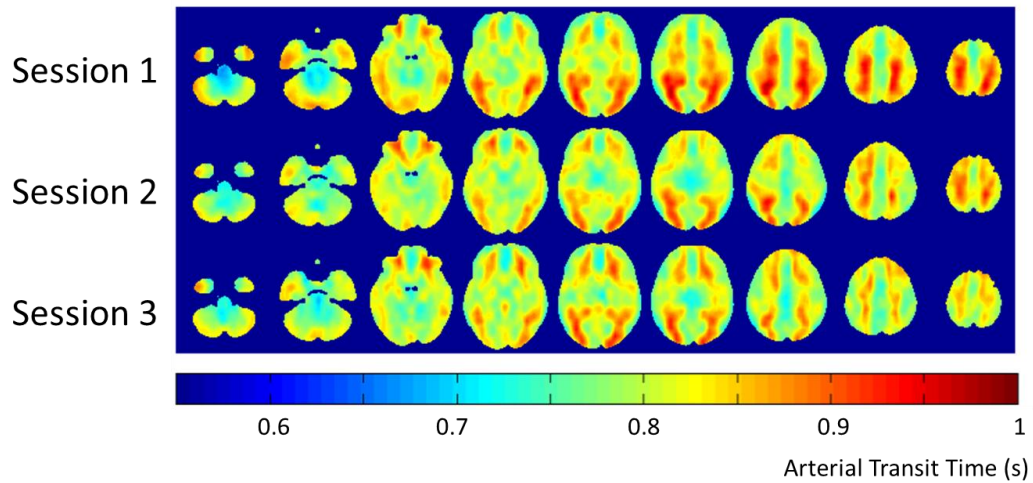


**Figure 3.5:** Group mean ATT maps (in seconds) for each session. (N=7)

The spatial patterns of the ATT maps were consistent across sessions, as demonstrated by the low between-session voxel-wise wsCV ( $5.0 \pm 2.7\%$ ). In a voxel-wise repeated measures ANOVA (implemented in SPM) testing for differences in ATT between sessions, no voxels survived the statistical threshold ( $p < .05$ , FWE). Variability between subjects was higher than between-sessions with mean grey matter wsCV equal to  $9.7 \pm 3.5\%$ . The between-subject maps showed increased variability in the medial regions of the brain, while cortical grey matter remained relatively homogeneous (Figure 3.5).

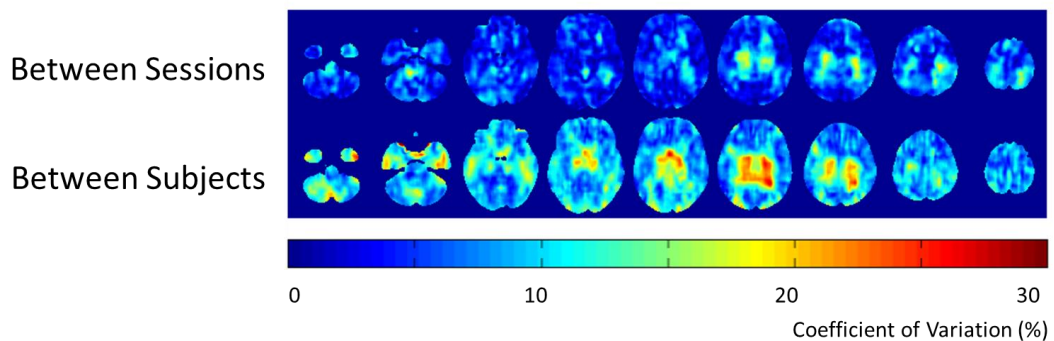


**Figure 3.6:** Between-sessions and between-subjects reproducibility of arterial transit times.

Since ATT values can vary based on the feeding artery, variability in ATT across the three main vascular territories was assessed. Mean ATT was the lowest in the ACA ( $796 \pm 3$  ms) followed by the PCA ( $812 \pm 8$  ms) and lastly, the MCA ( $817 \pm 7$  ms). Between the three sessions, there was no significant difference in the ATT. However, the ATT in the MCA was significantly higher from the value for the ACA territory ( $p < .05$ ).

### 3.5 Reproducibility of Motor Task Activation

Activation patterns generated from rest and task data sets from the same session and those generated from rest and task data acquired in sessions separated by a week and a month are shown in Figure 3.7. Results are presented for both aCBF and after normalizing each session's data by grey matter CBF (i.e. rCBF). Within-session activation represents the "best case" scenario since it is not affected by additional noise caused by repositioning errors and day-to-day variations in basal blood flow.

Since the task data remained the same in all comparisons, the within-session and between-session activation patterns should appear similar, provided these additional sources of noise were minimal. Regions in color represent voxels that survived the statistical threshold after correction for multiple comparisons using the FWE rate ( $p < .05$ ). There was good agreement in the spatial pattern of activation generated in within-session and between-session data, particularly after normalizing the perfusion images to grey matter CBF. In subjects 1 and 2, the diminished cluster size observed in aCBF between-session activation data relative to within-session data, is not observed when rCBF was used to generate activation. Interestingly, activation maps generated using aCBF for subjects 3 and 6 showed an increase in the size of activation in the motor regions in the between-sessions analysis compared to the original within-session analysis.

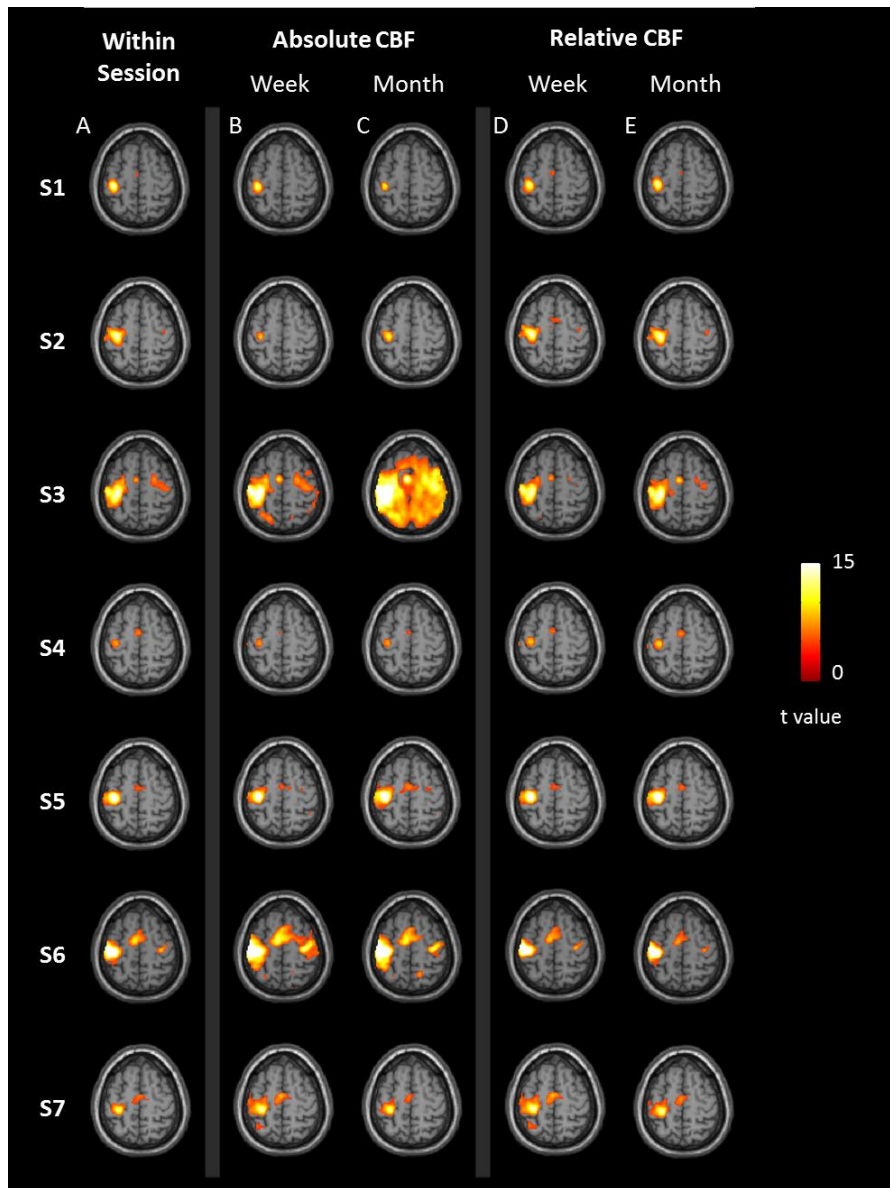


**Figure 3.7:** Areas of significant CBF increases associated with finger tapping overlaid on a T1-weighted MNI template brain. For each subject, activation maps were generated for: (a) within-session with aCBF rest and task data, (b) aCBF rest and task data separated by a week, (c) aCBF rest and task data separated by a month, (d) rCBF rest and task data separated by a week and (e) rCBF rest and task data separated by a month. Regions in colour represent voxels that survived the statistical threshold after correction for FWE ( $p < .05$ ). Data from the first run for subject 1 were excluded from this analysis since the task was not performed correctly.

Percent signal change within the motor cortex for run 1 and run 2 when rest and task were within the same session, separated by a week and separated by a month are shown in Table 3.6. There were no significant differences in the percent signal change within the primary motor cortex for any of the conditions using either absolute or relative CBF. However, the variability in the CBF response based on the analysis of the aCBF images was greater for the between-session analyses compared to the within-session analysis. This was caused by sizable day-to-day variations in resting CBF in some subjects, as evident for subject 3 in Figure 3.7. The results of the rCBF data show that this variability is considerably reduced by global normalization.

**Table 3.6:** Percent CBF change in the motor cortex during finger tapping averaged across all subjects. Results are reported separately for the two runs and for the within-session and between-session analyses

	Run 1			Run 2		
	Within Session	Between-Sessions Week	Between-Sessions Month	Within Session	Between-Sessions Week	Between-Sessions Month
<b>Absolute <math>\Delta</math>CBF (%)</b>	24.7 $\pm$ 8.6	21.0 $\pm$ 14.2	28.0 $\pm$ 15.8	20.2 $\pm$ 8.4	14.0 $\pm$ 12.8	17.2 $\pm$ 8.3
<b>Relative <math>\Delta</math>CBF (%)</b>		25.8 $\pm$ 8.1	25.2 $\pm$ 6.8		19.7 $\pm$ 10.2	19.5 $\pm$ 7.8

### 3.6 Precision of Motor Activation

Individual subject precision estimates based on the analysis of aCBF and rCBF data are shown in Figure 3.8. Data from the first run for subject 1 was excluded as discussed previously. Mean precision estimates from the within-session analysis and when the rest and task runs were separated by a week and by a month were  $93.9 \pm 11.0$ ,  $74.2 \pm 31.2$ , and  $65.0 \pm 32.7\%$  for aCBF, respectively, and  $94.5 \pm 12.1$ ,  $84.6 \pm 15.0$ , and  $78.5 \pm 15.2\%$  for rCBF, respectively. For the majority of subjects, the precision was higher for the rCBF analysis, particularly for subjects 3 and 6.

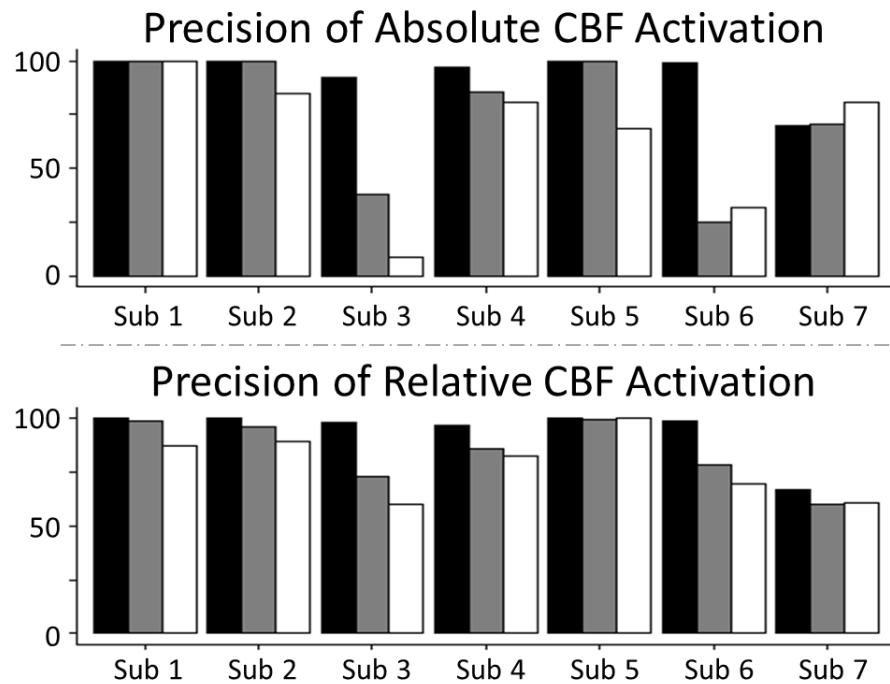


**Figure 3.8:** Precision measurements for each subject when rest and task data were from the same session (black), and when rest and task data were separated by a week (grey) or a month (white).

For both aCBF and rCBF data, there appeared to be a decline in precision as the separation between rest and task increased; however, this trend was only statistically significant for the rCBF data.

## Chapter 4

### 4 Discussion

The primary aim of my thesis was to investigate whether ASL has the sensitivity to detect longitudinal changes in CBF within an individual. This was achieved by: (1) assessing the within and between-session variability in resting CBF, (2) determining whether changes in ATT could confound longitudinal perfusion monitoring, and (3) as a proof of concept, I investigated the ability of ASL to detect motor activation when rest and task images were from the same session, and when they were separated by a week and a month.

Exploratory neuroimaging methods are advantageous for identifying regions of the brain affected by neurological disease, especially when there is little to no a priori knowledge. This is in contrast to the more widely used ROI-based analysis, in which average CBF values in predefined regions are compared. There are two main consequences that arise from this key difference. First, averaging over neighboring voxels reduces the effect of artifacts caused by realignment errors. In contrast, precise realignment is imperative for voxel-wise analysis in order to avoid false positive activation arising from spatial offsets. Secondly, because CBF is not spatially averaged when performing voxel-wise analysis, the sensitivity of the approach is diminished by additional noise sources when comparing images from separate sessions. Therefore, for successful exploratory analysis, it is critical to understand and manage the sources of noise<sup>124</sup>.

Within-session variability primarily comes from noise in the MR signal and subject motion, while between-session variability also includes physiological noise (i.e. differences in basal blood flow) and errors introduced by differences in head position between sessions<sup>99,100,125</sup>. Accurate alignment of images from different sessions is

challenging with ASL because of the relatively large size of the voxels ( $\sim 4 \times 4 \times 6 \text{ mm}^3$ ), which are typically used in order to improve SNR. Consequently slight alignment errors can lead to regional signal differences when comparing CBF images from separate sessions, and these can translate into false positive activation in the resulting statistical parametric map<sup>111</sup>. Evidence of this was shown in Figure 1.6 for a visually cued motor task paradigm in which false activation is easily identified as activation in brain regions not associated with the paradigm. For my work, a relatively simple approach was implemented to mitigate registration errors. A personalized head mold was generated for each subject, which was used in subsequent imaging sessions to replicate the position of the head from the first day. The effectiveness of this approach is evident in high-contrast structural MR images shown in Figure 3.1. Despite the fact that the images from sessions 2 and 3 were acquired one week and one month later, they appear nearly identical to the image acquired on the first day. This agreement is reflected in the similarity in the magnitude of the between-session and within-session transformation values (Table 3.2). The magnitude of the rotation and translation required to align images from the separate sessions were less than 3 mm and  $3^\circ$ , respectively. These results are a good indication that alignment errors when comparing functional images acquired on between days should be small, thus minimizing false positives in the activation maps<sup>115</sup>.

The benefits of minimizing variability in head position were evident by the agreement in the variability measurements for within- and between-session analyses. Average voxel-wise wsCV values for grey matter rCBF were  $4.7 \pm 4.5\%$  from the within-session analysis and  $5.7 \pm 4.4\%$  from the between-session analysis. Similarly, the reliability, as indicated by the ICC measurements, was excellent for both within-session ( $0.89 \pm 0.20$ ) and between-session analysis ( $0.84 \pm 0.12$ ). This agreement demonstrates that minimizing registration errors helped to substantially reduce additional variance when comparing CBF images from separate sessions. Despite the efforts to minimize



physiological noise in this study, it still contributed to the between-session variability. In comparison to wsCV for between-session rCBF analysis, the mean wsCV for aCBF was 75% higher and the corresponding ICC decreased from a rating of excellent ( $0.84 \pm 0.12$ ) to good ( $0.66 \pm 0.19$ ). This marked reduction in between-session reliability and reproducibility reflects the increased physiological noise caused by day-to-day variations in CBF associated with diurnal fluctuations and state of arousal<sup>39-41</sup>. Despite efforts to reduce these effects, these results highlight the challenges of accounting for all sources of variability. As a caveat, the within-session wsCV also improved after global normalization. This was likely caused by changes in wakefulness and breathing pattern during an imaging session<sup>42,43</sup>. Previous reproducibility studies have used ROIs to assess within- and between-session variability of resting CBF. For example, Mezue et al. demonstrated good between-session (week to month separation) reproducibility of resting grey matter CBF (wsCV 5.3 – 10.0%)<sup>24</sup>. Similarly, Wang et al. also showed high reproducibility with a wsCV of 5.7% in cortical grey matter<sup>44</sup>. The current study indicates that similar levels of can also be achieved at the voxel-wise level.

The reproducibility and reliability maps (Figure 3.3 and Figure 3.4) revealed spatial heterogeneity, particularly for the between-session analysis. The most noticeable feature was the higher variance in the centre of the head, which corresponds to midbrain regions such as the thalamus. It has been suggested that increased variability in thalamic activity is a reflection of variability in arousal<sup>82,130</sup>. Mezue et al. demonstrated that resting CBF in the thalamus decreased over 30 minutes, suggesting a decrease in attentional processing over time. However in the current study, it is unlikely that thalamic activity is the sole contributor to the increased variability as the area extends beyond its borders. A second, possibility is additional noise caused by geometric distortions in the images due to magnetic susceptibility artifacts in the intracranial cavities near the midbrain<sup>130</sup>. A third possibility, and the most likely in this study, is related to the 3D GRASE sequence.

Single-shot 3D imaging was implemented to provide fast acquisition with good spatial coverage, and SNR, which is advantageous for functional applications<sup>114,131</sup>. However, since raw image data were acquired within a single excitation with a long acquisition window due to T2 decay, it is prone to axial signal wrap-around and through-plane blurring<sup>43,132,133</sup>. The greater between-session variance observed in the centre of the head, resulting from z-direction blurring caused by pulsatile flow in large cerebral vessels located below the thalamus, could affect the results in applications of interest relating to midbrain regions. For example, chronic pain, where the thalamus plays a key role in the modulation of nociceptive information<sup>13,14</sup>. One possible solution would be to use a multi-shot 3D GRASE sequence to improve the phase encoding along the axial direction and reduce the acquisition window<sup>132,133</sup>.

Recent studies have identified spatial heterogeneity in ATTs as a confounder for measuring CBF accurately<sup>111,134</sup>. Although multi-PLD sequences have been used to image ATT and CBF simultaneously, the trade-off is suboptimal SNR for perfusion imaging and lengthy acquisitions<sup>76</sup>. In the current study, a low-resolution ATT sequence was implemented because ATT values differ based on large vascular territories<sup>109,134,135</sup>. The similarity in the appearance of group-wise ATT maps generated per session (Figure 3.5) and low between-sessions wsCV values (Figure 3.6) demonstrate that regional ATT values were consistent across time. In a repeated measures ANOVA that tested for differences across sessions, no voxels survived statistical threshold ( $p < .05$ , FWE). Likewise the between-session variability was low (wsCV < 10%). Average ATT values for the three sessions ( $806 \pm 45$ ,  $801 \pm 35$ , and  $796 \pm 39$  ms, respectively) were shorter than the implemented PLD (1.2 s). This indicates that there was sufficient time for labeled blood water to reach the imaging voxels prior to image acquisition. These results indicate that the ATT would not be a substantial confound in longitudinal CBF studies, at least in healthy individuals, provided the chosen PLD is within an optimal range. It would

be prudent to monitor ATT in longitudinal studies involving older subjects or patients with vascular disease, considering that low-resolution ATT images can be acquired within a few minutes<sup>76</sup>.

The similarity in the with-session and between-session measures of reproducibility and reliability indicate that ASL should have sufficient statistical power to detect longitudinal changes in regional CBF. To demonstrate this, statistical parametric mapping was performed on rest and motor activation ASL data sets from sessions separated by up to a month. This approach represents a proof of concept of the ability of ASL to detect low frequency activation, rather than the variability in activation measured across imaging sessions, which has been extensively studied<sup>54,82,98,136</sup>. From the within-session analysis, activation was detected in the primary motor cortex in all subjects and also in the supplementary motor cortex and the cerebellum in a few subjects (Figure 3.7). The similarities between these activation maps (i.e. the ground truth) and the corresponding maps generated using resting CBF data acquired one week and one month later demonstrate the ability of ASL to detect on a voxel-wise basis longitudinal changes in CBF. Visual inspection of the within and between-session activation maps generated before (aCBF) and after global normalization (rCBF) indicate that fluctuations in global CBF can significantly degrade the activation maps. This effect was most clearly illustrated in the 1 month aCBF activation map from subject 3. The large number of falsely identified activated voxels was caused by a 12.4 ml/100g/min change (or 26 % increase) in global CBF between the two imaging sessions. True activation in motor-related regions can still be identified by their larger t-scores relative to the values for the remainder of the brain. Normalizing the CBF images in each session by their corresponding global value substantially reduced the number of false positives (Figure 3.8), consequently the between-session rCBF activation maps appeared very similar to the original within-session activation maps (Figure 3.7).

Despite the remarkable similarities in the appearance of the within and between-session rCBF activation maps, displaying a single slice cannot properly assess the extent of false activation. Instead, the quality of the activation maps was characterized by measuring the precision, which was calculated from the number of true activation voxels in motor-related regions and the number of false activation voxels in the rest of the brain. Although this is a relative measure that depends on the extent of brain activation for the chosen task, it does provide a means of assessing the magnitude of false activation. Similar to the noise metrics, the precision was found to be lower for the between-session analysis compared to the within-session, and was better for the rCBF images compared to the aCBF images. Relative to the within-session activation, the precision decreased by 20% for aCBF images separated by a week and 30% for aCBF images separated by a month. As expected, global normalization improved the between-session precision. Relative to the within-session activation, the precision decreased by 10% for rCBF images separated by a week and 17% for rCBF images separated by a month. In other words, even with a month separation between rest and task, less than ~20% of activation detected would be false positives. Considering that the fraction of true activated voxels was 1% of the total number of grey matter voxels, these precision estimates highlight the ability of ASL to detect longitudinal changes in CBF, particularly if the confounding effects of variations in global CBF are removed.

The minimal CBF change in a given voxel that can be detected was calculated based on the standard paired samples t-test equation (i.e.  $\Delta\text{CBF}_{\min} = (\text{SD}_{\Delta\text{CBF}}/\sqrt{n})/t_{\text{crit}}$ ). The critical t-statistic ( $t_{\text{crit}}$ ) was estimated using the FWE corrected t-threshold generated by voxel-wise analysis,  $\text{SD}_{\Delta\text{CBF}}$  was calculated from the MATLAB implemented ANOVA and  $n$  is the number of perfusion images per run. For the within-session analysis, this threshold was approximately 3%, while for the between-session analysis it was 7% based on the variance measured for aCBF and 4% for rCBF. These thresholds are considerably smaller

than the 20 to 25% change in CBF measured in the motor cortex (Table 3.6), but are in-line with previous calculations<sup>15</sup>. The magnitude of the between-session thresholds indicate that ASL should be capable of detecting longitudinal changes in brain function, such as caused by pain<sup>137</sup>, which are associated with smaller CBF changes than those produced by a sensory task like finger tapping.

## Chapter 5

### 5 Summary

#### 5.1 Limitations and Future Work

These experiments represent an idealized situation; firstly, the subjects were young and healthy and secondly, a task paradigm with a predictable activation pattern and large effect size was used. Detection of regional changes in brain activity in clinical populations would pose a greater challenge considering there could be greater variability in the extent and magnitude of changes in regional CBF. Therefore there are a number of important implications to consider if a similar approach was used in a clinical population.

In this study ATTs were not found to have a substantial effect on the reproducibility of CBF. However, in older individuals and stroke patients this may not be the case. Studies have shown that cerebral vessels in older people are more tortuous and therefore the amount of time it takes for the label to reach the brain increases with age<sup>43</sup>. Furthermore, it could vary over time in patients with age and extent of vascular disease. Future studies involving older populations or patient populations are likely necessary to verify the suitability of ASL imaging with one PLD and to assess the stability of the ATTs over time.

The results of these experiments highlight the benefits of normalizing the CBF image by the global average; however, this approach should be implemented with caution. Normalizing in the presence of global systemic shifts between populations has been shown to alter group-wise differences<sup>126</sup>. It is unclear if normalization on an individual basis, such as performed in this study, would be affected in a similar manner the same

issues; however, one solution is to normalize the CBF images by a region considered unaffected by the disease <sup>101</sup>.

Despite high degree of alignment between sessions, the steps employed to reproduce the same head position across sessions were time consuming, adding on average an extra 30 minutes to the session. This is clearly suboptimal, particularly when dealing with patients who are less tolerant to long scan times (e.g., children, dementia patients) <sup>138</sup>. Realignment of the same imaging position in subsequent sessions requires the use of automatic alignment software. A recent multi-center study highlighted the capability of using such software to reposition subjects regardless of scanner location and operator <sup>103</sup>. Despite the involvement of 284 subjects and 28 centers, variability baseline CBF was low (the within-subject standard deviation was 5.3 ml/100g/min). For within session motion, self-navigation or prospective motion correction techniques (e.g. PROMO) where the pulse sequence is adjusted in real time based positioning of subject in scanner have shown promise. However, many of these are sequence specific. In some cases, they require additional hardware and are often implemented at the expense of increased scan time <sup>139-141</sup>.

Future considerations will be to implement a multi-shot 3D GRASE sequence to avoid smearing and wrap around effects. This is important for the study of chronic pain considering a number of midbrain regions are associated with pain perception and this is the area that demonstrated the highest between-session variability. In these experiments a relatively simple functional task with a well-defined pattern of activation was used as a proof of concept. Future experiments could involve a paradigm more closely related to the disease of interest such as an experimental pain stimulus. Another possibility would be to increase the time between rest and task sessions given that CBF monitoring over periods greater than a month would be needed to study disease progression or treatment

effects. For example, recovery of motor abilities in stroke patients extends beyond 30 days<sup>142</sup>.

## 5.2 Conclusion

This study demonstrated that ASL has the sensitivity to detect motor activation over periods extending up to a month within an individual. At the voxel-wise level, we demonstrate low variability in resting CBF, similar within- and between-session activation, and between-session precision of activation once the effects of basal blood flow were accounted for. In the young healthy population studied, ATT is not a substantial confound to the reproducibility of CBF measurements. Future investigations are required to assess the influence of ATT on the variability of CBF in clinical and older populations. These results demonstrate the feasibility of conducting voxel-wise analysis of CBF images acquired on different days and highlights the potential of this technique for voxel-wise longitudinal studies to assess changes in perfusion related to disease processes.



## References

1. Grichnik, K. P. & Ferrante, F. M. The difference between acute and chronic pain. *Mt. Sinai J. Med.* **58**, 217–220 (1991).
2. Pergolizzi, J. *et al.* The development of chronic pain: physiological CHANGE necessitates a multidisciplinary approach to treatment. *Curr. Med. Res. Opin.* **29**, 1127–35 (2013).
3. Merskey, H. & Bogduk, N. *Classification of Chronic Pain. Descr. Chronic Pain Defin. Pain Terms* (IASP press Seattle, 1994).
4. Moulin, D. E., Clark, A. J., Speechley, M. & Morley-Forster, P. K. Chronic pain in Canada--prevalence, treatment, impact and the role of opioid analgesia. *Pain Res. Manag.* **7**, 179–184 (2002).
5. Schopflocher, D., Taenzer, P. & Jovey, R. The prevalence of chronic pain in Canada. *Pain Res Manag* **16(6)**, 445–450 (2011).
6. Lynch, M. E. The need for a Canadian pain strategy. *Pain Res. Manag.* **16**, 77–80 (2011).
7. Choinière, M. *et al.* The Canadian STOP-PAIN project - Part 1: Who are the patients on the waitlists of multidisciplinary pain treatment facilities? *Can. J. Anesth.* **57**, 539–548 (2010).
8. Turk, D. C., Wilson, H. D. & Cahana, A. Treatment of chronic non-cancer pain. *Lancet* **377**, 2226–2235 (2011).
9. Coghill, R. C., McHaffie, J. G. & Yen, Y.-F. Neural correlates of interindividual differences in the subjective experience of pain. *Proc. Natl. Acad. Sci. U. S. A.* **100**, 8538–8542 (2003).
10. King, N. B., Fraser, V., Boikos, C., Richardson, R. & Harper, S. Determinants of increased opioid-related mortality in the united states and canada, 1990-2013: A systematic review. *Am. J. Public Health* **104**, (2014).
11. Apkarian, A. V., Bushnell, M. C., Treede, R.-D. & Zubieta, J.-K. Human brain mechanisms of pain perception and regulation in health and disease. *Eur. J. Pain* **9**, 463–84 (2005).
12. Voscopoulos, C. & Lema, M. When does acute pain become chronic? *Br. J. Anaesth.* **105**, i69–i85 (2010).

13. Fukumoto, M., Ushida, T., Zinchuk, V. S., Yamamoto, H. & Yoshida, S. Contralateral thalamic perfusion in patients with reflex sympathetic dystrophy syndrome. *Lancet* **354**, 1790–1791 (1999).
14. Ushida, T. *et al.* Alterations of contralateral thalamic perfusion in neuropathic pain. *Open Neuroimag. J.* **4**, 182–186 (2010).
15. Owen, D. G., Clarke, C. F., Ganapathy, S., Prato, F. S. & St. Lawrence, K. S. Using perfusion MRI to measure the dynamic changes in neural activation associated with tonic muscular pain. *Pain* **148**, 375–386 (2010).
16. Owen, D. G. *et al.* Measuring the neural response to continuous intramuscular infusion of hypertonic saline by perfusion MRI. *J. Magn. Reson. Imaging* **35**, 669–677 (2012).
17. Maleki, N., Brawn, J., Barmettler, G., Borsook, D. & Becerra, L. Pain response measured with arterial spin labeling. *NMR Biomed.* **26**, 664–673 (2013).
18. Hodkinson, D. J. *et al.* Quantifying the test-retest reliability of cerebral blood flow measurements in a clinical model of on-going post-surgical pain: A study using pseudo-continuous arterial spin labelling. *NeuroImage. Clin.* **3**, 301–310 (2013).
19. Kucyi, A. *et al.* Enhanced medial prefrontal-default mode network functional connectivity in chronic pain and its association with pain rumination. *J. Neurosci.* **34**, 3969–75 (2014).
20. Wise, R. G. *Neuroimaging Modalities: Description, Comparisons, Strengths and Weaknesses. Transl. neuroimaging; tools CNS drug Discov. Dev. Treat.* (Ringgold Inc, 2013).
21. Brooks, D. J. Positron emission tomography and single-photon emission computed tomography in central nervous system drug development. *NeuroRx* **2**, 226–236 (2005).
22. Morbelli, S. *et al.* The need of appropriate brain SPECT templates for SPM comparisons. *Q. J. Nucl. Med. Mol. Imaging* **52**, 89–98 (2008).
23. Della Rosa, P. A. *et al.* A Standardized [18F]-FDG-PET Template for Spatial Normalization in Statistical Parametric Mapping of Dementia. *Neuroinformatics* **12**, 575–593 (2014).
24. Gispert, J. D. *et al.* Influence of the normalization template on the outcome of statistical parametric mapping of PET scans. *Neuroimage* **19**, 601–612 (2003).

25. Ishii, K. *et al.* Statistical brain mapping of 18F-FDG PET in Alzheimer's disease: validation of anatomic standardization for atrophied brains. *J. Nucl. Med.* **42**, 548–557 (2001).
26. Zanotti-Fregonara, P. *et al.* Population-based input function and image-derived input function for [<sup>11</sup>C](R)-rolipram PET imaging: methodology, validation and application to the study of major depressive disorder. *Neuroimage* **63**, 1532–41 (2012).
27. Zanotti-Fregonara, P., Chen, K., Liow, J.-S., Fujita, M. & Innis, R. B. Image-derived input function for brain PET studies: many challenges and few opportunities. *J. Cereb. Blood Flow Metab.* **31**, 1986–1998 (2011).
28. Byrnes, K. R. *et al.* FDG-PET imaging in mild traumatic brain injury: A critical review. *Front. Neuroenergetics* **6**, (2014).
29. Yoder, K. K. *Basic PET Data Analysis Techniques*. (InTech, 2013). doi:10.5772/57126
30. Ogawa, S. & Lee, T. Brain magnetic resonance imaging with contrast dependent on blood oxygenation. *Proc. ...* **87**, 9868–72 (1990).
31. Thulborn, K. R., Waterton, J. C., Matthews, P. M. & Radda, G. K. Oxygenation Dependence of the Transverse Relaxation-Time of Water Protons in Whole-Blood at High-Field. *Biochim. Biophys. Acta* **714**, 265–270 (1982).
32. Detre, J. A. & Wang, J. Technical aspects and utility of fMRI using BOLD and ASL. *Clin. Neurophysiol.* **113**, 621–634 (2002).
33. Amaro, E. & Barker, G. J. Study design in fMRI: Basic principles. *Brain Cogn.* **60**, 220–232 (2006).
34. Wang, J. *et al.* Arterial spin labeling perfusion fMRI with very low task frequency. *Magn. Reson. Med.* **49**, 796–802 (2003).
35. Aguirre, G. K., Detre, J. A., Zarahn, E. & Alsop, D. C. Experimental design and the relative sensitivity of BOLD and perfusion fMRI. *Neuroimage* **15**, 488–500 (2002).
36. Logothetis, N. K. What we can do and what we cannot do with fMRI. *Nature* **453**, 869–878 (2008).
37. Xu, G. *et al.* Reliability and precision of pseudo-continuous arterial spin labeling perfusion MRI on 3.0 T and comparison with 15O-water PET in elderly subjects at risk for Alzheimer's disease. *NMR Biomed.* **23**, 286–293 (2010).

38. Petersen, E. T., Zimine, I., Ho, Y. C. L. & Golay, X. Non-invasive measurement of perfusion: A critical review of arterial spin labelling techniques. *Br. J. Radiol.* **79**, 688–701 (2006).
39. Hoogenraad, F. G. C. *et al.* Quantitative Differentiation Between BOLD Models in fMRI. *Most* **246**, 233–246 (2001).
40. Wu, W., Lawrence, K. S. S., Licht, P. D. J. & Wang, D. J. J. Quantification Issues in Arterial Spin Labeling Perfusion. *Magn. Reson. Imaging* **21**, 65–73 (2011).
41. Detre, J. a., Leigh, J. S., Williams, D. S. & Koretsky, A. P. Perfusion imaging. *Magn. Reson. Med.* **23**, 37–45 (1992).
42. Liu, T. T. & Brown, G. G. Measurement of cerebral perfusion with arterial spin labeling: Part 1. Methods. *J. Int. Neuropsychol. Soc.* **13**, 517–525 (2007).
43. Alsop, D. C. *et al.* Recommended implementation of arterial spin-labeled perfusion MRI for clinical applications: A consensus of the ISMRM perfusion study group and the European consortium for ASL in dementia. *Magn. Reson. Med.* **00**, (2014).
44. Wong, E. C. An introduction to ASL labeling techniques. *J. Magn. Reson. Imaging* **40**, 1–10 (2014).
45. Gevers, S., Majoie, C. B., van den Tweel, X. W., Lavini, C. & Nederveen, A. J. Acquisition time and reproducibility of continuous arterial spin-labeling perfusion imaging at 3T. *Am. J. Neuroradiol.* **30**, 968–71 (2009).
46. Jahng, G., Li, K., Ostergaard, L. & Calamante, F. Perfusion Magnetic Resonance Imaging : A Comprehensive Update on Principles and Techniques. **15**, 554–577 (2014).
47. Chuang, K. *et al.* Mapping resting-state functional connectivity using perfusion MRI. *Neuroimage* **40**, 1595–1605 (2009).
48. Hernandez-Garcia, L., Lee, G. R., Vazquez, A. L. & Noll, D. C. Fast Pseudo-Continuous Arterial Spin Labeling for Functional Imaging Using a Two-Coil System. *Magn. Reson. Med.* **51**, 577–585 (2004).
49. Liu, J. *et al.* Quantitative cerebral blood flow mapping and functional connectivity of postherpetic neuralgia pain: A perfusion fMRI study. *Pain* **154**, 110–118 (2013).
50. Du, T. *et al.* Hypoperfusion in frontotemporal dementia and Alzheimer disease by arterial spin labeling MRI. *Neurology* **67**, 1215–1220 (2006).

51. Alsop, D. C., Dai, W., Grossman, M. & Detre, J. a. Arterial spin labeling blood flow MRI: Its Role in the early characterization of Alzheimer's disease. *J. Alzheimer's Dis.* **20**, 871–880 (2010).
52. Hartkamp, N. S., van Osch, M. J. P., Kappelle, J. & Bokkers, R. P. H. Arterial spin labeling magnetic resonance perfusion imaging in cerebral ischemia. *Curr. Opin. Neurol.* **27**, 42–53 (2014).
53. Chalela, J. A. *et al.* Magnetic Resonance Perfusion Imaging in Acute Ischemic Stroke Using Continuous Arterial Spin Labeling. *Stroke* **31**, 680–687 (2000).
54. Vilela, P., Pimentel, M., Sousa, I. & Figueiredo, P. Quantification of perfusion changes during a motor task using arterial spin labeling. *Neuroradiol. J.* **24**, 85–91 (2011).
55. Poudel, G. R., Innes, C. R. H. & Jones, R. D. Cerebral Perfusion Differences Between Drowsy and Nondrowsy Individuals After Acute Sleep Restriction. *Sleep* **35**, 1085–1096 (2012).
56. Mutsaerts, H. J. M. M. *et al.* Reproducibility of pharmacological ASL using sequences from different vendors: implications for multicenter drug studies. *Magn. Reson. Mater. Physics, Biol. Med.* (2015). doi:10.1007/s10334-014-0480-1
57. Klomp, a, Caan, M. W. a, Denys, D., Nederveen, a J. & Reneman, L. Feasibility of ASL-based phMRI with a single dose of oral citalopram for repeated assessment of serotonin function. *Neuroimage* **63**, 1695–700 (2012).
58. Franklin, T. R. *et al.* Modulation of resting brain cerebral blood flow by the GABA B agonist, baclofen: a longitudinal perfusion fMRI study. *Drug Alcohol Depend.* **117**, 176–83 (2011).
59. Chen, J. J., Wieckowska, M., Meyer, E. & Pike, G. B. Cerebral blood flow measurement using fMRI and PET: A cross-validation study. *Int. J. Biomed. Imaging* **2008**, (2008).
60. Zhang, K. *et al.* Comparison of cerebral blood flow acquired by simultaneous [(15)O]water positron emission tomography and arterial spin labeling magnetic resonance imaging. *J. Cereb. Blood Flow Metab.* 1–8 (2014). doi:10.1038/jcbfm.2014.92
61. Cha, Y.-H. K. *et al.* Regional correlation between resting state FDG PET and pCASL perfusion MRI. *J. Cereb. Blood Flow Metab.* **33**, 1909–14 (2013).
62. Wong, E. C., Buxton, R. B. & Frank, L. R. Implementation of quantitative perfusion imaging techniques for functional brain mapping using pulsed arterial spin labeling. *NMR Biomed.* **10**, 237–249 (1997).

63. Edelman, R. R. & Chen, Q. EPSTAR MRI: multislice mapping of cerebral blood flow. *Magn. Reson. Med.* **40**, 800–805 (1998).
64. Kim, S. G. Quantification of Relative Cerebral Blood-Flow Change By Flow-Sensitive Alternating Inversion-Recovery (Fair) Technique - Application To Functional Mapping. *Magn. Reson. Med.* **34**, 293–301 (1995).
65. Williams, D. S., Detre, J. A., Leigh, J. S. & Koretsky, a P. Magnetic resonance imaging of perfusion using spin inversion of arterial water. *Proc. Natl. Acad. Sci. U. S. A.* **89**, 212–216 (1992).
66. Utting, J. F., Thomas, D. L., Gadian, D. G. & Ordidge, R. J. Velocity-driven adiabatic fast passage for arterial spin labeling: Results from a computer model. *Magn. Reson. Med.* **49**, 398–401 (2003).
67. Hernandez-Garcia, L., Lewis, D. P., Moffat, B. & Branch, C. A. Magnetization Transfer Effects on the Efficiency of Flow-driven Adiabatic Fast Passage Inversion of Arterial Blood. *NMR Biomed.* **20**, 733–742 (2010).
68. Zaharchuk, G. *et al.* Multislice perfusion and perfusion territory imaging in humans with separate label and image coils. *Magn. Reson. Med.* **41**, 1093–1098 (1999).
69. Dai, W., Garcia, D., de Bazelaire, C. & Alsop, D. C. Continuous flow-driven inversion for arterial spin labeling using pulsed radio frequency and gradient fields. *Magn. Reson. Med.* **60**, 1488–97 (2008).
70. Buxton, R. B. *et al.* A General Kinetic Model for Quantitative Perfusion Imaging with Arterial Spin Labeling. *Magn. Reson. Med.* **40**, 383–396 (1998).
71. Herscovitch, P. & Raichle, M. E. What is the correct value for the brain-blood partition coefficient for water? *J. Cereb. Blood Flow Metab.* **5**, 65–69 (1985).
72. Parkes, L. M. & Tofts, P. S. Improved accuracy of human cerebral blood perfusion measurements using arterial spin labeling: Accounting for capillary water permeability. *Magn. Reson. Med.* **48**, 27–41 (2002).
73. Aslan, S. *et al.* Estimation of Labeling Efficiency in Pseudo-Continupus Arterial Spin Labeling. *Magn. Reson. Med.* **63**, 765–771 (2011).
74. Alsop, D. C. & Detre, J. A. Reduced transit-time sensitivity in noninvasive magnetic resonance imaging of human cerebral blood flow. *J. Cereb. Blood Flow Metab.* **16**, 1236–1249 (1996).

75. MacIntosh, B. J. *et al.* Assessment of arterial arrival times derived from multiple inversion time pulsed arterial spin labeling MRI. *Magn. Reson. Med.* **63**, 641–647 (2010).
76. Dai, W., Robson, P. M., Shankaranarayanan, A. & Alsop, D. C. Reduced resolution transit delay prescan for quantitative continuous arterial spin labeling perfusion imaging. *Magn. Reson. Med.* **67**, 1252–1265 (2012).
77. Shrout, P. E. & Fleiss, J. L. Intraclass correlations: Uses in assessing rater reliability. *Psychol. Bull.* **86**, 420–428 (1979).
78. Fleiss, J. L., Levin, B. A. & Paik, M. C. *Statistical methods for rates and proportions*. **3rd**, (Wiley, 2003).
79. Weir, J. P. Quantifying Test-Retest Reliability Using the Intraclass Correlation Coefficient and the SEM. *J. Strength Cond. Res.* **19**, 231–240 (2005).
80. Bennett, C. M. & Miller, M. B. How reliable are the results from functional magnetic resonance imaging? *Ann. N. Y. Acad. Sci.* **1191**, 133–155 (2010).
81. Bartlett, J. W. & Frost, C. Reliability, repeatability and reproducibility: analysis of measurement errors in continuous variables. *Ultrasound Obstet. Gynecol.* **31**, 466–475 (2008).
82. Mezue, M. *et al.* Optimization and reliability of multiple postlabeling delay pseudo-continuous arterial spin labeling during rest and stimulus-induced functional task activation. *J. Cereb. Blood Flow Metab.* 1–9 (2014). doi:10.1038/jcbfm.2014.163
83. Chen, Y., Wang, D. J. J. & Detre, J. A. Comparison of arterial transit times estimated using arterial spin labeling. *Magn. Reson. Mater. Physics, Biol. Med.* **25**, 135–144 (2012).
84. Bland, J. M. & Altman, D. G. Measurement error proportional to the mean. *Br. Med. J.* **313**, 106 (1996).
85. Parkes, L. M., Rashid, W., Chard, D. T. & Tofts, P. S. Normal cerebral perfusion measurements using arterial spin labeling: reproducibility, stability, and age and gender effects. *Magn. Reson. Med.* **51**, 736–43 (2004).
86. Fawcett, T. An introduction to ROC analysis. *Pattern Recognit. Lett.* **27**, 861–874 (2006).
87. Tracey, I. & Bushnell, M. C. How Neuroimaging Studies Have Challenged Us to Rethink: Is Chronic Pain a Disease? *J. Pain* **10**, 1113–1120 (2009).

88. Wasan, A. D. *et al.* Neural correlates of chronic low back pain measured by arterial spin labeling. *Anesthesiology* **115**, 364–374 (2011).
89. Ellis, N. & Large, B. The early stages of reading: A longitudinal study. *Appl. Cogn. Psychol.* **2**, 47–76 (1988).
90. Szaflarski, J. P. *et al.* A longitudinal functional magnetic resonance imaging study of language development in children 5 to 11 years old. *Ann. Neurol.* **59**, 796–807 (2006).
91. Aguirre, G. K. & Detre, J. A. The development and future of perfusion fMRI for dynamic imaging of human brain activity. *Neuroimage* **62**, 1279–1285 (2012).
92. Thirion, B. *et al.* Analysis of a large fMRI cohort: Statistical and methodological issues for group analyses. *Neuroimage* **35**, 105–120 (2007).
93. Edelstein, W. a, Glover, G. H., Hardy, C. J. & Redington, R. W. The intrinsic signal-to-noise ratio in NMR imaging. *Magn. Reson. Med.* **3**, 604–618 (1986).
94. Krüger, G., Kastrup, A. & Glover, G. H. Neuroimaging at 1.5 T and 3.0 T: Comparison of oxygenation-sensitive magnetic resonance imaging. *Magn. Reson. Med.* **45**, 595–604 (2001).
95. Jezzard, P. *Physiological Noise: Strategies for Correction. Funct. MRI* (Springer-Verlag, 1999). doi:10.1016/j.mri.2003.08.020
96. Gorgolewski, K. J., Storkey, A. J., Bastin, M. E., Whittle, I. & Pernet, C. Single subject fMRI test-retest reliability metrics and confounding factors. *Neuroimage* **69**, 231–43 (2013).
97. Jahng, G.-H. *et al.* Human Brain : Reliability and Reproducibility of Pulsed Arterial. *Radiology* 909–916 (2005).
98. Raoult, H. *et al.* Arterial spin labeling for motor activation mapping at 3T with a 32-channel coil: Reproducibility and spatial accuracy in comparison with BOLD fMRI. *Neuroimage* **58**, 157–167 (2011).
99. Floyd, T. F., Ratcliffe, S. J., Wang, J., Resch, B. & Detre, J. a. Precision of the CASL-perfusion MRI technique for the measurement of cerebral blood flow in whole brain and vascular territories. *J. Magn. Reson. Imaging* **18**, 649–55 (2003).
100. Chen, Y., Wang, D. J. J. & Detre, J. a. Test-retest reliability of arterial spin labeling with common labeling strategies. *J. Magn. Reson. Imaging* **33**, 940–9 (2011).
101. Aslan, S. & Lu, H. On the sensitivity of ASL MRI in detecting regional differences in cerebral blood flow. *Magn. Reson. Imaging* **28**, 928–35 (2010).



102. Gevers, S. *et al.* Intra- and multicenter reproducibility of pulsed, continuous and pseudo-continuous arterial spin labeling methods for measuring cerebral perfusion. *J. Cereb. Blood Flow Metab.* **31**, 1706–15 (2011).
103. Petersen, E. T., Mouridsen, K. & Golay, X. The QUASAR reproducibility study, Part II: Results from a multi-center Arterial Spin Labeling test-retest study. *Neuroimage* **49**, 104–13 (2010).
104. Jiang, L. *et al.* Reliability and reproducibility of perfusion MRI in cognitively normal subjects. *Magn. Reson. Imaging* **28**, 1283–1289 (2010).
105. Heijtel, D. F. R. *et al.* Accuracy and precision of pseudo-continuous arterial spin labeling perfusion during baseline and hypercapnia: a head-to-head comparison with <sup>15</sup>O H<sub>2</sub>O positron emission tomography. *Neuroimage* **92**, 182–92 (2014).
106. Henriksen, O. M. *et al.* Estimation of intersubject variability of cerebral blood flow measurements using MRI and positron emission tomography. *J. Magn. Reson. Imaging* **35**, 1290–1299 (2012).
107. Mutsaerts, H. J. M. M. *et al.* Multi-vendor reliability of arterial spin labeling perfusion MRI using a near-identical sequence: Implications for multi-center studies. *Neuroimage* **113**, 143–152 (2015).
108. Kuhn, F. P. *et al.* Comparison of PET template-based and MRI-based image processing in the quantitative analysis of C11-raclopride PET. *EJNMMI Res.* **4**, 7 (2014).
109. Sousa, I., Vilela, P. & Figueiredo, P. Reproducibility of the quantification of arterial and tissue contributions in multiple postlabeling delay arterial spin labeling. *J. Magn. Reson. Imaging* **40**, 1453–62 (2013).
110. Petr, J. *et al.* Template-based approach for detecting motor task activation-related hyperperfusion in pulsed ASL data. *Hum. Brain Mapp.* **35**, 1179–89 (2014).
111. Borogovac, A., Habeck, C., Small, S. a & Asllani, I. Mapping brain function using a 30-day interval between baseline and activation: a novel arterial spin labeling fMRI approach. *J. Cereb. Blood Flow Metab.* **30**, 1721–33 (2010).
112. Witt, S. T., Laird, A. R. & Meyerand, M. E. Functional neuroimaging correlates of finger-tapping task variations: An ALE meta-analysis. *Neuroimage* **42**, 343–356 (2008).
113. Mathew, R. J. & Wilson, W. H. Substance abuse and cerebral blood flow. *Am. J. Psychiatry* **148**, 292–305 (1991).

114. Günther, M., Oshio, K. & Feinberg, D. a. Single-shot 3D imaging techniques improve arterial spin labeling perfusion measurements. *Magn. Reson. Med.* **54**, 491–8 (2005).
115. Wang, Z. *et al.* Empirical optimization of ASL data analysis using an ASL data toolbox: ASLtbx. *Magn. Reson. Imaging* **26**, 261–269 (2009).
116. Fischmeister, F. P. S. *et al.* The benefits of skull stripping in the normalization of clinical fMRI data. *NeuroImage. Clin.* **3**, 369–80 (2013).
117. Ashburner, J. & Friston, K. J. Unified segmentation. *Neuroimage* **26**, 839–851 (2005).
118. Wang, J. *et al.* Arterial transit time imaging with flow encoding arterial spin tagging (FEAST). *Magn. Reson. Med.* **50**, 599–607 (2003).
119. Lu, H., Clingman, C., Golay, X. & Van Zijl, P. C. M. Determining the longitudinal relaxation time (T1) of blood at 3.0 tesla. *Magn. Reson. Med.* **52**, 679–682 (2004).
120. Chappell, M. a., Groves, a. R., Whitcher, B. & Woolrich, M. W. Variational Bayesian Inference for a Nonlinear Forward Model. *IEEE Trans. Signal Process.* **57**, 223–236 (2009).
121. Woolrich, M. W. *et al.* Bayesian analysis of neuroimaging data in FSL. *Neuroimage* **45**, S173–S186 (2009).
122. Bland, J. M. & Altman, D. G. Measurement error proportional to the mean. *BMJ* **313**, 106 (1996).
123. Tatu, L., Moulin, T., Bogousslavsky, J. & Duvernoy, H. Arterial territories of the human brain: cerebral hemispheres. *Neurology* **50**, 1699–1708 (1988).
124. Greve, D. N. *et al.* Cortical Surface-based Analysis Reduces Bias and Variance in Kinetic Modeling of Brain PET Data. **127**, 358–366 (2012).
125. Jahng, G. *et al.* Human Brain: Reliability and Reproducibility of Pulsed Arterial Spin-labeling Perfusion MR Imaging. *Radiology* **234**, 909–916 (2005).
126. Borghammer, P. *et al.* Normalization in PET group comparison studies--the importance of a valid reference region. *Neuroimage* **40**, 529–40 (2008).
127. Diamant, M., Harms, M. P. M., Immink, R. V., Van Lieshout, J. J. & Van Montfrans, G. a. Twenty-four-hour non-invasive monitoring of systemic haemodynamics and cerebral blood flow velocity in healthy humans. *Acta Physiol. Scand.* **175**, 1–9 (2002).

128. Ramsay, S. C. *et al.* Changes in global cerebral blood flow in humans: effect on regional cerebral blood flow during a neural activation task. *J. Physiol.* **471**, 521–534 (1993).
129. Ainslie, P. N. & Duffin, J. Integration of cerebrovascular CO<sub>2</sub> reactivity and chemoreflex control of breathing: mechanisms of regulation, measurement, and interpretation. *Am. J. Physiol. Regul. Integr. Comp. Physiol.* **296**, R1473–R1495 (2009).
130. Wang, Y. *et al.* Regional reproducibility of pulsed arterial spin labeling perfusion imaging at 3T. *Neuroimage* **54**, 1188–95 (2011).
131. Fernández-Seara, M. a. *et al.* Minimizing acquisition time of arterial spin labeling at 3T. *Magn. Reson. Med.* **59**, 1467–1471 (2008).
132. Vidorreta, M. *et al.* Comparison of 2D and 3D single-shot ASL perfusion fMRI sequences. *Neuroimage* **66**, 662–71 (2013).
133. Huan Tan, W. Scott Hoge, Craig A. Hamilton, Matthias Günther, R. A. K. 3D GRASE PROPELLER: Improved Image acquisition Technique for Arterial Spin Labelling Perfusion Imaging. **66**, 168–173 (2014).
134. MacIntosh, B. J. *et al.* Multiple inflow pulsed arterial spin-labeling reveals delays in the arterial arrival time in minor stroke and transient ischemic attack. *Am. J. Neuroradiol.* **31**, 1892–1894 (2010).
135. Borogovac, A. Novel Method for Superior Detection of Functional Changes in CBF using Arterial Spin Labeling fMRI Ajna Borogovac Submitted in partial fulfillment of the requirements for the degree of Doctoral of Philosophy in the Graduate School of Arts and Sciences COL. (2010).
136. Steketee, R. M. E. *et al.* Quantitative Functional Arterial Spin Labeling (fASL) MRI – Sensitivity and Reproducibility of Regional CBF Changes Using Pseudo-Continuous ASL Product Sequences. *PLoS One* **10**, e0132929 (2015).
137. Howard, M. a *et al.* Beyond patient reported pain: perfusion magnetic resonance imaging demonstrates reproducible cerebral representation of ongoing post-surgical pain. *PLoS One* **6**, e17096 (2011).
138. Liu, J. Z., Zhang, L., Brown, R. W. & Yue, G. H. Reproducibility of fMRI at 1.5 T in a strictly controlled motor task. *Magn. Reson. Med.* **52**, 751–60 (2004).
139. Maclaren, J., Herbst, M., Speck, O. & Zaitsev, M. Prospective motion correction in brain imaging: A review. *Magn. Reson. Med.* **69**, 621–636 (2013).

140. White, N. *et al.* PROMO: Real-time prospective motion correction in MRI using image-based tracking. *Magn. Reson. Med.* **63**, 91–105 (2010).
141. Zun, Z., Shankaranarayanan, A. & Zaharchuk, G. Pseudocontinuous arterial spin labeling with prospective motion correction (PCASL-PROMO). *Magn. Reson. Med.* **1056**, 1049–1056 (2013).
142. Duncan, P. W., Goldstein, L. B., Matchar, D., Divine, G. W. & Feussner, J. Measurement of motor recovery after stroke. *Stroke* **23**, 1084–1089 (1992).

## Appendices

### Appendix A: Ethics Approval Notice



Research Ethics

Use of Human Participants - Ethics Approval Notice

**Principal Investigator:** Dr. Keith St. Lawrence  
**File Number:**2653  
**Review Level:**Delegated  
**Approved Local Adult Participants:**104  
**Approved Local Minor Participants:**0  
**Protocol Title:**Technical Development of Functional Magnetic Resonance Imaging Techniques at 1.5 and 3 Tesla. (REB #11412)  
**Department & Institution:**Schulich School of Medicine and Dentistry\Lawson Health Research Institute, Lawson Health Research Institute  
**Sponsor:**  
**Ethics Approval Date:**May 14, 2013 **Expiry Date:**December 31, 2015  
**Documents Reviewed & Approved & Documents Received for Information:**

Document Name	Comments	Version Date
Revised Study End Date		

This is to notify you that The University of Western Ontario Research Ethics Board for Health Sciences Research Involving Human Subjects (HSREB) which is organized and operates according to the Tri-Council Policy Statement: Ethical Conduct of Research Involving Humans and the Health Canada/ICH Good Clinical Practice Practices: Consolidated Guidelines; and the applicable laws and regulations of Ontario has reviewed and granted approval to the above referenced revision(s) or amendment(s) on the approval date noted above. The membership of this REB also complies with the membership requirements for REB's as defined in Division 5 of the Food and Drug Regulations.

The ethics approval for this study shall remain valid until the expiry date noted above assuming timely and acceptable responses to the HSREB's periodic requests for surveillance and monitoring information. If you require an updated approval notice prior to that time you must request it using the University of Western Ontario Updated Approval Request Form.

Members of the HSREB who are named as investigators in research studies, or declare a conflict of interest, do not participate in discussion related to, nor vote on, such studies when they are presented to the HSREB.

The Chair of the HSREB is Dr. Joseph Gilbert. The HSREB is registered with the U.S. Department of Health & Human Services under the IRB registration number IRB 00000940.

**Appendix B:** Copyright license for Figure 1.5**JOHN WILEY AND SONS LICENSE  
TERMS AND CONDITIONS**

Nov 02, 2015

---

This Agreement between Tracy Ssali ("You") and John Wiley and Sons ("John Wiley and Sons") consists of your license details and the terms and conditions provided by John Wiley and Sons and Copyright Clearance Center.

License Number	3680360009063
License date	Aug 01, 2015
Licensed Content Publisher	John Wiley and Sons
Licensed Content Publication	Magnetic Resonance in Medicine
Licensed Content Title	Arterial spin labeling perfusion fMRI with very low task frequency
Licensed Content Author	Jiongjiong Wang,Geoffrey K. Aguirre,Daniel Y. Kimberg,Anne C. Roc,Lin Li,John A. Detre
Licensed Content Date	Apr 15, 2003
Pages	7
Type of Use	Dissertation/Thesis
Requestor type	University/Academic
Format	Print and electronic
Portion	Figure/table
Number of figures/tables	1
Original Wiley figure/table number(s)	Figure 2
Will you be translating?	No
Title of your thesis / dissertation	Feasibility of Arterial Spin Labeling for Detection of Longitudinal Activation
Expected completion date	Aug 2015
Expected size (number of pages)	85

## Appendix C: Copyright license for Figure 1.6

### NATURE PUBLISHING GROUP LICENSE TERMS AND CONDITIONS

Nov 02, 2015

This is an Agreement between Tracy Ssali ("You") and Nature Publishing Group ("Nature Publishing Group"). It consists of your order details, the terms and conditions provided by Nature Publishing Group, and the payment terms and conditions.

All payments must be made in full to CCC. For payment instructions, please see information listed at the bottom of this form.

License Number	3680351165566
License date	Aug 01, 2015
Licensed Content Publisher	Nature Publishing Group
Licensed Content Publication	Journal of Cerebral Blood Flow & Metabolism
Licensed Content Title	Mapping brain function using a 30-day interval between baseline and activation: a novel arterial spin labeling fMRI approach
Licensed Content Author	Ajna Borogovac, Christian Habeck, Scott A Small and Iris Aslani
Licensed Content Date	Jul 21, 2010
Volume number	30
Issue number	10
Type of Use	reuse in a dissertation / thesis
Requestor type	academic/educational
Format	print and electronic
Portion	figures/tables/illustrations
Number of figures/tables /illustrations	1
High-res required	no
Figures	Figure 5
Author of this NPG article	no
Your reference number	None
Title of your thesis / dissertation	Feasibility of Arterial Spin Labeling for Detection of Longitudinal Activation
Expected completion date	Aug 2015
Estimated size (number of pages)	85

## Curriculum Vitae

### TRACY SSALI

---

<b>Post-secondary Education and Degrees</b>	<p>The University of Western Ontario London, Ontario, Canada 2009-2013 B.MSc.</p> <p>The University of Western Ontario London, Ontario, Canada 2009-2013 M.Sc.</p>
<b>Honours and Awards</b>	<p>Western Graduate Student Scholarship The University of Western Ontario 2013 - 2015</p> <p>Deans List The University of Western Ontario 2009 – 2012</p> <p>Craig R. Williams Scholarship Loblaw Companies Limited 2010 - 2011</p> <p>Western Scholarship of Excellence The University of Western Ontario 2009 – 2010</p>
<b>Publications</b>	<p>Anazodo UC, Thiessen JD, <b>Ssali Tracy</b>, Mandel J, Günther M, Butler J, Pavlosky W, Prato FS, Thompson RT and St. Lawrence KS. Feasibility of simultaneous wholebrain imaging on an integrated PET-MRI system using an enhanced 2-point Dixon attenuation correction method. <i>Frontiers in Neuroscience</i>. (2015)</p>
<b>Oral Presentations</b>	<p><b>Ssali Tracy</b>, Anazodo UC, Shokouhi M, MacIntosh BJ, and St Lawrence K. Intra and Intersubject Reproducibility of Arterial Transit Time. <i>International Society for Magnetic Resonance in Medicine</i>, Toronto, Canada (06/2015)</p>



**Poster  
Presentations**

**Ssali Tracy**, Anazodo UC, Bureau Y, Butler J, Günther M, and St Lawrence K. Feasibility of Arterial Spin Labeling for Detection of Longitudinal Cerebral Blood Flow Changes. Brain, Vancouver, Canada (06/2015 – 06/2015)

**Ssali Tracy**, Anazodo UC, Bureau Y, Butler J, Günther M, and St Lawrence K. Feasibility of Arterial Spin Labeling for Detection of Low Frequency Activation. Imaging Network Ontario, London, Canada. (03/2015)

**Ssali Tracy**, Anazodo UC, Bureau Y, Butler J, Günther M, and St Lawrence K. Feasibility of Arterial Spin Labeling for Detection of Low Frequency Activation. (04/2015)  
London Health Research Day, London, Canada

**Ssali Tracy**, Shokouhi M, Anazodo UC, Butler J, St Lawrence KS. Detection of Inter- Sessional Functional Activation by Arterial Spin Labeling. Organization of Human Brain Mapping, Hamburg, Germany (06/2014)

Anazodo UC, **Ssali Tracy**, Mandel J, Butler J, Gunther M, Prato F, Terry T, St Lawrence KS. Simultaneous investigation of regional CBF and glucose metabolism with 3D- pCASL and 18[F]-FDG. Organization of Human Brain Mapping, Hamburg, Germany (06/2014)

**Ssali Tracy**, Shokouhi M, Anazodo UC, Butler J, St Lawrence KS. Detection of Inter-Sessional Functional Activation by Arterial Spin Labeling. London Imaging Discovery, London, Canada (06/2014)

Anazodo U, Shoemaker J, **Ssali Tracy**, Wang D, Suskin N, St Lawrence K. Age-Related Cerebrovascular Reactivity with and without Partial Volume Correction. International Society for Magnetic Resonance in Medicine. Amsterdam, Netherlands (10/2012)

**Related Work  
Experience**

Undergraduate Research Assistant  
National Research Council Canada, London Ontario  
09/2012 - 05/2013  
Supervisor: Dr. Gord Campbell and Dr. Terry Thompson

Undergraduate Research Assistant  
Lawson Health Research Institute, London Ontario  
01/2012 – 08/2013  
Supervisor: Dr. Keith St Lawrence